AN ABSTRACT OF THE THESIS OF

Ryan P. Longman for the degree of Master of Science in Wood Science and Civil Engineering presented on December 8, 2021.

Title: In-plane Creep Behavior of Cross-laminated Timber and Mass Plywood Panels: A Methodology to Evaluate the Long-term Performance of Post-Tensioned Mass Timber Walls

Abstract approved:

_____

Mariapaola Riggio Yelda Turkan

Post-tensioned (PT) self-centering shear walls were designed to reduce structural damage from seismic activity. However, these lateral force resistant systems experience post-tension loss negatively affecting the re-centering capability due to delayed deformations experienced by engineered wood products over time. The long-term mechanical response of mass-timber panels to in-plane PT loads is a complex, multi-physics problem involving moisture diffusion, constrained hygroexpansion, and viscoelastic and mechano-sorptive response of the panel to the PT load, which is mitigated by the deformation of the panel. Changes in the relative humidity of the surrounding environment affects the wood moisture content and results in additional creep due to the mechano-sorptive effect. Methodologies developed to accurately measure creep and post-tension loss and improve the visualization of monitoring these phenomena in an existing building to-date proved insufficient.

Therefore, a new methodology was developed to measure viscoelastic and mechano-sorptive creep characteristics of small-scale post-tensioned cross-laminated timber (CLT) and mass plywood panel (MPP) wall specimens in two controlled environments. The combined data from these tests will be useful for updating PT loss

modeling parameters, or to create a new predictive creep model. Additionally, a full-scale monitoring study of 28 ft tall post-tensioned CLT and MPP walls was proposed to obtain long-term data from a structural system and validate the model. The model will then be used to predict PT losses in a real building based on input data obtained from a structural health monitoring (SHM) system.

Furthermore, to streamline SHM, measurands including relative humidity, air and wood temperature, wood moisture content, displacements and deformations of shear walls, and tensile force of post-tensioned rods, were integrated and visualized in a Building Information Model (BIM), as it enables the storage of spatial information, including building geometry and dimensions, and non-spatial attributes, such as material type and sensor readings. The approach intends to simplify the necessary steps required to create a digital model of a structure linked to historical sensor data to improve the visualization of SHM data to assist with maintenance decisions. Specifically, the BIM was proposed to access all the environmental and structural monitored parameters used to describe and predict the long-term response of mass timber post-tensioned shear walls in a building. The east stairwell of the George W. Peavy Forest Science Center ("Peavy Hall") at Oregon State University was used as a case study to test the proposed approach. Since there was no accurate, as-built BIM available, the BIM of PT CLT shear walls was developed using a Scan-to-BIM approach by converting Light Detection and Ranging (LiDAR) point clouds into a BIM. All sensors included in the BIM were linked to their historical data displayed on the internet and easily accessible through a list that highlights their locations within the digital model. The precise placement of these sensors and the possibility to associate the measured parameters of these entities within a BIM is hypothesized to assist with data management by adding a spatial element to data and analysis results, which could lead to a more streamlined maintenance and service life planning of a building.

The creep tests, modeling, full-scale monitoring of post-tensioned systems, and BIM for SHM were developed to assist with the design and maintenance of post-tensioned timber shear walls. The creep tests were designed to capture important data such as load, viscoelastic creep, mechano-sorptive creep, timber moisture content,

environmental conditions, and timber shrinkage and swelling, useful for refining material properties to create a predictive model. The creep model currently accounts for the creep of CLT under a constant load, which is a preliminary step towards predicting the post-tension loss of PT shear walls. In future work, the data recorded from the tests should be analyzed to update the creep model to include mechano-sorptive effects and a varying load due to PT loss. Engineers can benefit from a predictive model to design a system that reduces and accounts for expected PT loss, so the building remains seismically resilient. Building managers and occupants of a building can benefit through the improved visualization of SHM data. A future study can incorporate the live sensory data into the BIM and display the data for the public. This would allow occupants to make maintenance requests and be aware of future maintenance tasks that can improve the service life of the building.

In-plane Creep Behavior of Cross-laminated Timber and Mass Plywood Panels: A Methodology to Evaluate the Long-term Performance of Post-tensioned Mass Timber Walls

by
Ryan P. Longman

A THESIS

submitted to

Oregon State University

in partial fulfillment of
the requirements for the
degree of

Master of Science

Presented December 8, 2021
Commencement June 2022

Master of Science thesis of Ryan P. Longman presented on December 8, 2021

APPROVED:

Co-Major Professor, representing Wood Science and Engineering

Co-Major Professor, representing Civil Engineering

Head of the Department of Wood Science and Engineering

Head of the School of Civil and Construction Engineering

Dean of the Graduate School

I understand that my thesis will become part of the permanent collection of Oregon State University libraries. My signature below authorizes release of my thesis to any reader upon request.

Ryan P. Longman, Author

ACKNOWLEDGEMENTS

Thank you to Drs. Mariapaola Riggio, Lech Muszynski, André Barbosa, and Yelda Turkan for their support and guidance throughout this project. I am so grateful for my graduate experience with you all as my mentors. I appreciate your positive attitudes during an unpredictable year.

Thank you to Esther Baas for her strong work ethic, organization skills, and willingness to help with all tasks. This project would not be a success without her.

Thank you to Gabriele Granello for his enthusiasm and insight involved with this project. Thank you to Dr. John Nairn for his guidance during creep modeling.

Thank you to Tyler Deboodt, Byrne Miyamoto, and Milo Clauson for their brainstorming and help with lab activities.

Thank you to Dylan Willard for being a great friend, workout buddy, and roommate, even though we disagree on how to load the dishwasher. Thank you to Ian Morrell, Kenneth Udele, Mohit Srivastava, Sujit Bhandari, Matthias Wind, Maria Munoz, Evan Schmidt, and Sina Jahedi for being involved with the Forest Utilization Society club (FUSe).

Thank you to Nada Albader and Emily Davis for their help with lab activities.

Thank you to Freres Lumber, DR Johnson, Hexion, Andersen Construction, and Simpson Strong-Tie for providing materials for this project.

Thank you to the College of Forestry and School of Civil and Construction Engineering for supporting this project. This study was funded by the “Design, construction, and maintenance of mass timber PT shear walls” conducted through the TallWood Design Institute with funding by the U.S. Department of Agriculture’s Agricultural Research Service (USDA ARS) Agreement No. 58-0204-9-165. The material presented is also based upon work supported by the National Institute of Food and Agriculture, U.S. Department of Agriculture, McIntire Stennis project under 1009740 and the Achievement Rewards for College Scientists (ARCS).

CONTRIBUTION OF AUTHORS

Chapter 1 and 2 introductory topics and research motivation were identified, developed, and refined with contributions from Dr. Mariapaola Riggio, Dr. Lech Muszynski, Dr. André Barbosa, Dr. Gabriele Granello, Dr. Yelda Turkan, and Esther J. Baas.

Chapter 3 was developed from the *Numerical modeling of in-plane creep behavior of post-tensioned mass timber wall panels* conference paper presented at the World Conference on Timber Engineering WCTE-2021. Dr. Mariapaola Riggio, Dr. Lech Muszynski, Dr. André Barbosa, Dr. Gabriele Granello, Dr. John Nairn, and Esther J. Baas are co-authors of this paper. Dr. John Nairn developed the creep modeling software and incorporated the appropriate equations. The other co-authors contributed to the research ideas and background information.

Dr. Mariapaola Riggio, Dr. Lech Muszynski, Dr. André Barbosa, Dr. Gabriele Granello, and Esther J. Baas, contributed to the design of the experimental study described within Chapter 4. In addition, Esther J. Baas and Dr. André Barbosa provided structural designs and drawings for the specimens.

Chapter 5 was developed from the *Towards a digital twin for monitoring in-service performance of post-tensioned self-centering cross-laminated timber shear walls* conference paper presented at the ASCE 2021 International Conference on Computing in Civil Engineering (i3CE 2021). Esther J. Baas, Dr. Yelda Turkan and Dr. Mariapaola Riggio are co-authors of this paper and contributed to the research development. Dr. Yelda Turkan, Esther J. Baas, and Dr. Erzhuo Che assisted with collecting and processing the LiDAR data. Esther J. Baas, Dr. Mariapaola Riggio, and Dr. André Barbosa provided the preliminary structural health monitoring sensors and data that made this work possible.

TABLE OF CONTENTS

1 INTRODUCTION 1

1.1 Motivation 1
1.2 Research Objectives 3
1.3 Thesis Outline 5

2 BACKGROUND 6

2.1 Mass Timber Panels 6
2.2 Post-tensioned Timber Shear Walls 7
2.3 Post-tension Loss 9
2.3.1 Wood Moisture Content 9
2.3.2 Relaxation 10
2.3.3 Creep 10
2.3.4 Viscoelastic Creep 10
2.3.5 Mechano-sorptive Creep 11
2.4 Wood Creep Studies 13
2.5 The Material Point Method 15
2.6 Structural Health Monitoring 16
2.7 Building Information Modeling 16
2.8 Digital Twins and Digital Shadows 17

3 NUMERICAL MODELING OF IN-PLANE COMPRESSIVE CREEP BEHAVIOR OF CROSS-LAMINATED TIMBER 19

3.1 Introduction 19
3.1.1 Transverse Isotropy 19
3.1.2 Moisture Modeling 20
3.1.3 Viscoelasticity 21
3.2 3D Anisotropic Viscoelasticity Modeling Method 22
3.3 Results 26
3.3.1 Proposal for Modeling Mechano-sorption 28
3.4 Conclusions, Limitations, and Future Work 29

TABLE OF CONTENTS (Continued)

4 POST-TENSIONED SELF-CENTERING CROSS-LAMINATED TIMBER AND MASS PLYWOOD PANELS CREEP TEST DESIGNS AND METHODOLOGIES 31

4.1 Introduction 31
4.2 Materials and Methods 32
4.3 Small-scale Creep Test Methodologies 32
4.3.1 Constant Environment Creep Test 33
4.3.2 Varying Environment Creep Test 33
4.3.3 Small-scale Specimen Designs 34
4.3.4 Small-scale Cross-laminated Timber Specimens 35
4.3.5 Small-scale Mass Plywood Panel Specimens 39
4.4 Methodology for Monitoring Full-scale Post-tensioned Timber Walls 42
4.4.1 Full-scale Cross-laminated Timber Wall Design 45
4.4.2 Full-scale Mass Plywood Panel Wall Design 45
4.5 Conclusions 50

5 TOWARDS A DIGITAL TWIN FOR MONITORING IN-SERVICE PERFORMANCE OF POST-TENSIONED SELF-CENTERING CROSS-LAMINATED TIMBER SHEAR WALLS 51

5.1 Introduction 51
5.1.1 Structural Health Monitoring 51
5.1.2 Building Information Modeling 52
5.1.3 Digital Twins 54
5.2 Methodology for Creating a Building Information Model for Structural Health Monitoring 55
5.3 Case Study: The George W. Peavy Forest Science Center 57
5.4 Conclusions, Limitations, and Future Work 66

6 OVERALL CONCLUSIONS, LIMITATIONS, AND FUTURE WORK 68

6.1 Conclusions 68
6.2 Limitations 69
6.3 Future Work 70

TABLE OF CONTENTS (Continued)

7 BIBLIOGRAPHY 71

LIST OF FIGURES

Figure Page

Figure 1.1. Overall research outline of the project entitled “Design, construction and maintenance of mass timber PT shear walls: data, models and recommendations”. The blue frame includes the design activities developed within this thesis. 4

Figure 2.1. CLT rocking shear wall diagram (Source: StructureCraft, OSU Peavy Building) 8

Figure 2.2. Tensioned rods secured by hex nuts protruding out of CLT shear walls at Peavy Hall, Oregon, USA. 8

Figure 2.3. Three phases of creep: 1) primary, 2) secondary, and 3) tertiary (adapted from Granello and Palermo 2019). 11

Figure 2.4. Hydrogen bonds breaking and reforming at new sites between cellulose chains in the Grossman model (adapted from Schanzlin 2010). 13

Figure 2.5. Creep, relaxation, and post-tensioned mass timber walls visualized through force and deflection rates (credit: L. Muszynski). 14

Figure 3.1. The MPM model (solid) fitted to the experiments of Hu and Guan (dashed). 27

Figure 3.2. Output file from OSParticulas showing the material properties for wood as an isotropic material 28

Figure 4.1. Small-scale creep tests listed with measurands including loading conditions, environment, and creep deformations 33

Figure 4.2. Elevation view of the small-scale CLT specimen design (credit: E. Baas) 36

Figure 4.3. Section view of the small-scale CLT specimen design (credit: E. Baas). 37

Figure 4.4. Plan view of small-scale CLT specimens (credit: E. Baas) 38

Figure 4.5. Small-scale CLT specimen attached to a crane as a safety precaution. ... 38

Figure 4.6. Elevation view of the small-scale MPP specimen design (credit: E. Baas). 40

LIST OF FIGURES (Continued)

Figure 4.7. Section view of the small-scale MPP specimen design (credit: E. Baas) 41

Figure 4.8. Plan view of small-scale MPP specimens (credit: E. Baas) 42

Figure 4.9. Erected MPP (left) and CLT (right) walls during instrumentation of rods, LVDTs, and targets 44

Figure 4.10. Full-scale monitoring of post-tensioned systems occurs as free-standing walls and the post-tensioned walls in an existing building..... 45

Figure 4.11. Drawings of the full-scale CLT wall with elevation and section views (credit: E. Baas) 47

Figure 4.12. Plan view of CLT wall (credit: E. Baas) 48

Figure 4.13. Plan view of MPP wall (credit: E. Baas)..... 48

Figure 4.14. Drawings of the full-scale MPP wall with elevation and section views (credit: E. Baas) 49

Figure 5.1. Sensors placed on PT CLT walls in Peavy Hall, Oregon, USA. 58

Figure 5.2. Target locations used to register the point clouds to become a cohesive model..... 59

Figure 5.3. Building Information Model (left) and point cloud model (right) 60

Figure 5.4. Levels created by picking points within the virtual model..... 61

Figure 5.5. Point cloud fits within existing BIM for comparison and verification of correct units..... 61

Figure 5.6. Materials contain additional information under the Properties tab regarding the grade, dimensions, and comments 62

Figure 5.7. Point cloud view shows sensors in east stairwell 63

Figure 5.8. Sensor names are specified under the Specialty Equipment category 63

LIST OF FIGURES (Continued)

Figure 5.9. Sensor specifications provided by a link to the table that displays the measuring range and tolerance for all the sensors in the building (OSF 2021) 64

Figure 5.10. The Specialty Equipment Schedule in Revit lists all modeled sensors, the URL to see their data, a link to a table that provides sensor model specifications, and comments 65

Figure 5.11. The selected load cell in the Specialty Equipment Schedule becomes highlighted in the model (bottom left). Clicking on the URL within the schedule displays the sensor data in a new window (right). 66

DEDICATION

This thesis is dedicated to Djali, my neighbor’s dog.

1 INTRODUCTION

1.1 Motivation

Mass timber panels such as cross-laminated timber (CLT) and mass plywood panels (MPP) are innovative engineered wood products (EWPs) that enable the construction of mid- and high-rise timber buildings. In the United States, the growth is further supported by the 2021 International Building Code (IBC) approving mass timber structures up to 18 stories tall (AWC 2021).

While the IBC based timber structure designs allow for seismic designs that in the event of an extreme earthquake have life safety as their primary objective, the new horizon is resilient low-damage designs which aim to reduce seismic damage and accelerate post-event re-occupancy. Post-tensioned (PT) self-centering shear walls utilizing mass timber panels are a type of resilient, low-damage lateral force resisting system (LFRS), developed recently in New Zealand and in the United States (Palermo et al. 2005; Pei et al. 2019; Baas et al. 2021). Structural elements post-tensioned with unbonded steel rods, or tendons, accommodate the seismic demand through controlled rocking between the structural elements and through elastic steel elongation to re-center the structure after an earthquake with limited and localized structural damage (Pei et al. 2019). The effectiveness of the system relies on the tensile load in the tendons remaining at the prescribed level when the seismic event occurs.

However, data from monitored operative post-tensioned timber buildings in the United States (Baas et al. 2020b), New Zealand (Granello and Palermo 2020), and Europe (Granello et al. 2019) found that post-tensioned losses occurred at rates beyond expected values. PT losses are defined as the reduction in tension force after the rods or tendons are tensioned. Large tension losses can activate the rocking motion at lower intensity earthquakes, creating damage to non-structural elements, or negatively affecting the re-centering capability (Granello et al. 2020; Baas et al. 2020a; Granello et al. 2019; Granello and Palermo 2019).

The aforementioned monitoring studies (Baas et al. 2020b, Granello and Palermo 2020, Granello et al. 2019) suggest that PT losses depend on several parameters such as: anchorage details, the initial level of tension forces, and

environmental conditions. These parameters encompass the design of the LFRS system, tensioning of the rods during construction, and maintenance of the system as it is exposed to environmental conditions. The primary sources of PT losses in timber LFRS systems are steel relaxation, time-dependent creep in wood, and mechano-sorptive creep imposed by changes in the wood moisture content.

Modeling the creep deformation and its response to tension loss is important for predicting the long-term creep deformation of post-tensioned mass timber wall panels and its impact on tension loss to assess initial post-tensioning procedures and if, or when, the timber panels should be re-tensioned so their self-centering ability can be maintained for seismic resiliency.

A creep model needs to account for viscoelastic creep, mechano-sorptive creep, shrinkage and swelling deformations, timber moisture content, load, and environmental conditions. For the model to have predictive capabilities, there is a need to experimentally identify the creep behavior of CLT and MPP and evaluate the effects of exposure to a variable environment. The material parameters gathered from a creep test typically assume constant loading conditions, since it is difficult to determine them in tests where both the load and deformation vary. To evaluate the behavior of a post-tensioned structure, however, it is necessary to consider that the load is not constant due to post-tension losses. In addition, environmental conditions may vary seasonally and daily, thus affecting the creep rate and consequently tension loss.

While monitoring mass timber PT structures provides useful information of varying conditions affecting the long-term performance of these systems, stakeholders interested in the design, construction, and maintenance of PT buildings may have limited access to this information. Building information modeling (BIM) has been used to streamline the coordination of tasks during various stages of a project delivery. However, the use of BIM to access information and coordinate tasks during the service life of buildings, thus assisting with their condition control and maintenance planning, remains largely unexplored.

Building information models linked with monitoring data from the actual structure can be referred to as a form of digital twins (Lu et al. 2019). If the data from

the physical system do not dynamically update the digital model, it is referred to as a digital shadow (Sepasgozar 2021). Both approaches have potential for assisting with the service life management of novel structural systems, such as mass timber post-tensioned shear walls.

There is a need to for predicting the PT losses in mass timber buildings based on design, material properties and expected environmental exposure conditions. Material parameters are needed to predict the in-plane viscoelastic and mechano-sorptive creep of CLT and MPP. In addition, the entangled effects of creep and tension loss in an uncontrolled and realistic environment need to be analyzed. Lastly, access to long-term data of PT structures can be improved to assist with their life cycle management.

1.2 Research Objectives

The objectives of this research are to:

1) Create a preliminary model designed to measure the creep of a mass timber panel subjected to a constant load.
2) Develop a methodology that outlines the specific steps and requirements to measure the in-plane creep of CLT and MPP under constant and varying environmental conditions, to derive the material parameters for the predictive model.
3) Develop a methodology for monitoring the entangled effects of creep and tension loss in an uncontrolled and realistic environment by testing full-scale post-tensioned CLT and MPP wall panels.
4) Present a methodology and case study for creating a BIM to assist with visualizing data on the long-term performance of post-tensioned mass timber shear walls within a building.

To accomplish these research objectives, the research project was divided into numerous tasks. The creep of CLT was modeled using the Material Point Method (MPM), a modeling approach that has a few advantages over finite element analysis. Creep tests were developed for small-scale CLT and MPP PT systems in a constant

environment and an environment where the relative humidity fluctuates. A monitoring study was developed to record the PT loss and creep deformations of full-scale PT CLT and MPP walls in an uncontrolled environment. Lastly, a methodology was presented for scan-to-BIM to digital shadow for visualizing structural health monitoring (SHM) data for PT timber walls within a building.

This thesis aims to contribute to a research project entitled "Design, construction and maintenance of mass timber PT shear walls: data, models and recommendations" to evaluate the long-term behavior of post-tensioned self-centering rocking shear walls made using cross-laminated timber and mass plywood panels.

Figure 1.1 displays the thesis tasks (in the blue frame) within the general plan and workflow of the research project. The diagram displays tasks to collect the data gathered from the small-scale tests connected to the material model that is updated and refined by the full-scale PT elements and validated against actual PT loss data generated through monitored buildings. A more detailed description of these tasks is provided in the following section and in the related thesis chapters.

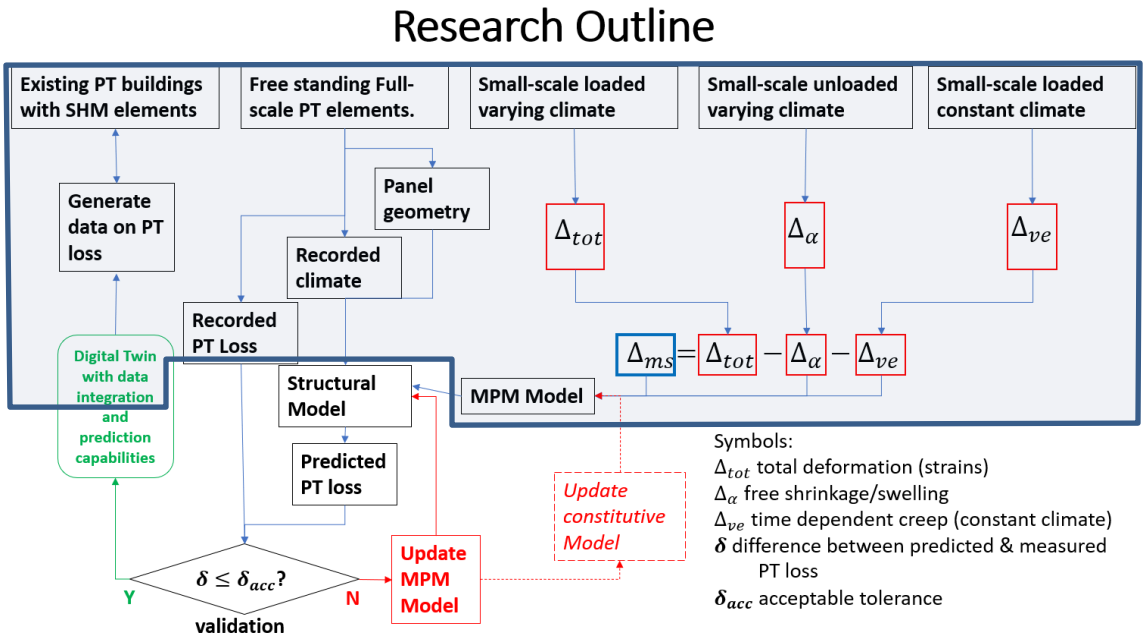

Figure 1.1. Overall research outline of the project entitled "Design, construction and maintenance of mass timber PT shear walls: data, models and recommendations". The blue frame includes the design activities developed within this thesis.

1.3 Thesis Outline

This thesis is comprised of six chapters. Chapter 2 provides an overview of the studied structural system and the phenomena affecting its long-term behavior. It also introduces the use of structural health monitoring and the concept of digital twins to assist with the service life management of mass timber systems. Chapter 3 focuses on numerical modeling of the in-plane compressive creep behavior of CLT. The material properties in the longitudinal direction and transverse directions were fit to creep test results from Hu and Guan 2018. Chapter 4 discusses the methodology developed to measure viscoelastic creep in small-scale post-tensioned CLT and MPP wall specimens in controlled environments so viscoelastic creep, mechano-sorptive creep, and shrinkage and swelling effects are separated. Next, a methodology is proposed for monitoring full-scale post-tensioned CLT and MPP walls in an uncontrolled environment to record the interactions between the variables within a structural system. Chapter 5 discusses the scan-to-BIM approach for creating a building information model (BIM) to assist with SHM data visualization of post-tensioned timber walls in the form of a digital shadow. Lastly, Chapter 6 provides overall conclusions, limitations, and future work.

2 BACKGROUND

Overview

The following chapter provides a background for understanding the products, structural system, and phenomena studied in this thesis. A definition of wood viscoelastic creep and mechano-sorptive creep is provided based on selected studies. This, far from being an exhaustive review of research done on these topics, lays the ground to the numerical study and the experimental plan described in the next chapters. This chapter also introduces concepts related to the development of digital twins and digital shadows. A digital shadow is considered a preliminary step towards the implementation of improved tools to assist with condition control of the studied systems.

2.1 Mass Timber Panels

Mass timber panels such as cross-laminated timber (CLT) and mass plywood panels (MPP) are innovative engineered wood products (EWPs) that enable the construction of mid- and high-rise timber buildings. The APA defines a CLT panel as "several layers of kiln-dried lumber boards stacked in alternating directions, bonded with structural adhesives, and pressed to form a solid, straight, rectangular panel," (APA 2021). Mass plywood panels are a large-scale, structural composite veneer-based engineered wood product produced by Freres Lumber Company, Inc in Lyons, Oregon, USA. MPP panels consist of multiple structural composite lumber layers pressed together with structural grade adhesive (Freres Lumber Co. 2021). Advantages of CLT and MPP compared to traditional solid-sawn lumber include enhanced dimensional stability, mechanical properties, and resource utilization. Both products are certified under ANSI/APA PRG 320 (2019). When compared to traditional steel and concrete construction, these EWPs offer shorter construction times due to pre-fabricated elements such as wall and floor panels, a higher strength-to-weight ratio, and lower carbon footprint.

Cross-laminated timber demand is expected to grow by over 13% annually into the mid-2020s (Beyreuther et al. 2017). In the United States, the growth is further

supported by the 2021 International Building Code (IBC) approving mass timber structures up to 18 stories tall (AWC 2021).

2.2 Post-tensioned Timber Shear Walls

While the IBC based timber structure designs provide guidelines for seismic designs that in the event of an extreme earthquake have life safety as their primary objective, the new horizon is resilient low-damage designs which aim to reduce seismic damage and accelerate post-event re-occupancy. One of the resilient, low-damage lateral force resisting systems (LFRS), developed in 2010 in New Zealand and also applied in the United States, uses EWPs with post-tensioned (PT) self-centering shear walls (Figure 2.1 and 2.2) (Palermo et al. 2005; Pei et al. 2019; Baas et al. 2021a). Structural elements post-tensioned with unbonded steel rods, or tendons, accommodate the seismic demand through controlled rocking between the structural elements and through elastic steel elongation to re-center the structure after an earthquake with no unintended structural damage (Pei et al. 2019). Extensive testing in the last 15 years gave rise to eleven low-damage LFRS timber building constructed between New Zealand, the United States, and Japan (Baas et al. 2021a; Granello et al. 2020).

With the introduction of mass timber PT LFRSs, a series of large-scale tests have been conducted, including a shake table test conducted at the Natural Hazards Engineering Research Infrastructure (NHERI) at the University of California, San Diego (Pei et al. 2019) informing and verifying the designs of PT timber walls. Laminated veneer lumber (LVL), cross-laminated timber (CLT), and glue laminated timber (glulam) are currently the only post-tensioned EWPs used in practice (Granello et al. 2020).

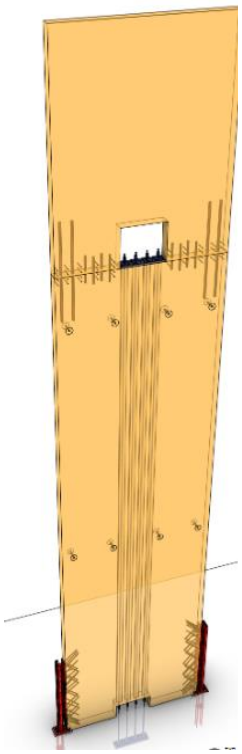

Figure 2.1. CLT rocking shear wall diagram (Source: StructureCraft, OSU Peavy Building)

Figure 2.2. Tensioned rods secured by hex nuts protruding out of CLT shear walls at Peavy Hall, Oregon, USA.

2.3 Post-tension Loss

The effectiveness of a PT system relies on the tensile load in the tendons remaining at the prescribed lever when a seismic event occurs (Smith et al. 2014). Post-tension losses are defined as the reduction in tension force after the rods or tendons are tensioned. All buildings with post-tensioned timber elements have experienced post-tension loss (Granello et al. 2018). Large tension losses can activate the rocking motion at lower intensity earthquakes, creating damage to non-structural elements, or negatively affecting the re-centering capability (Granello et al. 2020; Baas et al. 2020a; Granello at al. 2019; Granello and Palermo 2019).

Despite the extensive literature on the dynamic performance of PT structures, limited data is available on the PT losses over time. Limited data from monitored operative post-tensioned timber buildings in the United States (Baas et al. 2020b), New Zealand (Granello and Palermo 2020), and Europe (Granello et al. 2019) suggest that PT losses depend on several parameters such as: anchorage details, the initial level of tension forces, and environmental conditions. The primary sources of PT losses in timber LFRS systems are steel relaxation, time-dependent creep in wood, and mechano-sorptive creep imposed by changes in the wood moisture content.

2.3.1 Wood Moisture Content

Moisture content is defined as the mass of water in wood divided by the oven-dry mass of wood (Skaar 1988). Wood is a hygroscopic material that reacts to changes in its surrounding environment. The level of moisture content at which dimensional changes are first observed is called the “intersection point” or referred to as the fiber saturation point (FSP). A moisture content change below the FSP results in abrupt changes in the physical properties of wood such as electrical conductivity, mechanical strength, diffusivity, and density (Autengruber et al. 2021). Relative humidity and temperature of the ambient air are the two most important variables affecting the equilibrium moisture content (EMC) in wood where the moisture content is the same as the relative humidity of the surrounding air (Skarr 1983).

The service-life of timber systems can be negatively impacted by an increase in wood moisture content due to the climate or exposure to water. An increase in

wood moisture content can result in swelling, strength reduction, increased creep, and increases the likelihood of decay fungi and pests when the moisture content surpasses 15% (Skarr 1988, Glass 2010).

2.3.2 Relaxation

Relaxation is defined as a time-dependent reduction of internal reaction forces in materials or structural elements subjected to fixed deformation (Muszynski 2021). In a post-tensioned system, the steel rods begin relaxation after they are tensioned, reducing the compressive force along the steel bearing plates and timber wall panel.

2.3.3 Creep

Creep is the increased deformation of a member under a constant stress, like those generated by a permanent load. Wood and EWPs are viscoelastic materials where creep is a complex combination of irreversible deformations akin to viscous flow, and reversible deformations in the form of a delayed elastic behavior. A viscoelastic material is one that when subjected to stress, exhibits deformation behavior that can be described with a combination of models developed for an elastic solid and viscous fluid.

The structural performance of timber structures is significantly affected by the combination of mechanical loading and moisture content changes in response to the variations of ambient climate conditions. Timber structures may experience deformations due to loads, moisture content changes, and time. The creep deformation of timber elements can be separated into time-dependent creep, also referred to as viscoelastic creep, and mechano-sorptive creep (Toratti 1992).

2.3.4 Viscoelastic Creep

Viscoelastic creep is a time-dependent deformation of materials or structural elements under a constant load (Muszynski 2021). A wood member deforms elastically when initially loaded. If the load is constant, additional time-dependent deformation occurs. Creep is often characterized by creep rate or the change of creep deformation over time. It can be divided into three main phases (Findley and Davis 2013), as shown in Figure 2.3:

1. Primary creep: the deformation rapidly increases before reaching a more stable rate;
2. Secondary creep: the rate of deformation is fairly constant;
3. Tertiary creep: the deformation rate rapidly increases, leading to the failure of the material.

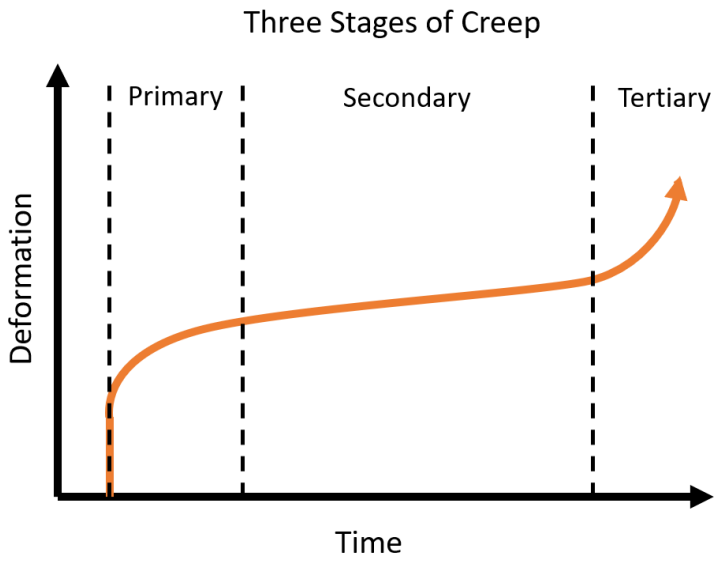

Figure 2.3. Three phases of creep: 1) primary, 2) secondary, and 3) tertiary (adapted from Granello and Palermo 2019).

2.3.5 Mechano-sorptive Creep

Mechano-sorptive creep is a deformation in timber structural elements subjected to sustained loads and exposed to variable service conditions with significant moisture changes below the fiber saturation point (Muszynski 2021). The mechano-sorptive effect is an additional deformation that cannot be attributed to simple superposition of elastic deformation, free shrinkage or swelling, or creep in steady climate conditions (Muszynski et al. 2005). The mechano-sorptive phenomenon was first reported by Armstrong and Kingston (1960) who described it as an acceleration in creep by a varying moisture content. Mechano-sorptive creep depends on changes in moisture content, unlike viscoelastic creep which is directly dependent on time. Any change in moisture content below the FSP results in an increase of creep, regardless of whether

the change is due to sorption or desorption (Grossman 1976, Hoffmeyer & Davidson 1989, Hunt 1991, and Toratti 1992).

Many conceptual models exist to better explain viscoelastic creep and mechano-sorptive creep in timber. Schanzlin (2010) summarized three conceptual models for creep behavior given by Grossman (1978), Boyd (1982), and Hoffmeyer and Davidson (1989), but the Grossman model is the most widely accepted explanation. In the Grossman model (1978), hydrogen bonds between polymeric constituents of wood cell walls break and reform with adjacent molecule chains. Cellulose molecule chains are interconnected by hydrogen bonds. The strength of individual bonds depend on the relative distance between hydroxyl (-OH) groups in adjacent cellulose chains. Primary bonds formed between hydroxyl groups in intimate contact are considered the strongest and most stable, while those formed over a distance larger than one Van der Waals radius, referred to as secondary bonds, are weaker and may be easily disrupted. The secondary bonds are temporarily broken during the removal or uptake of water. When the wood reaches equilibrium at a new moisture content, the hydrogen bonds are reformed at new sites, shown in Figure 2.4 (Schanzlin 2010).

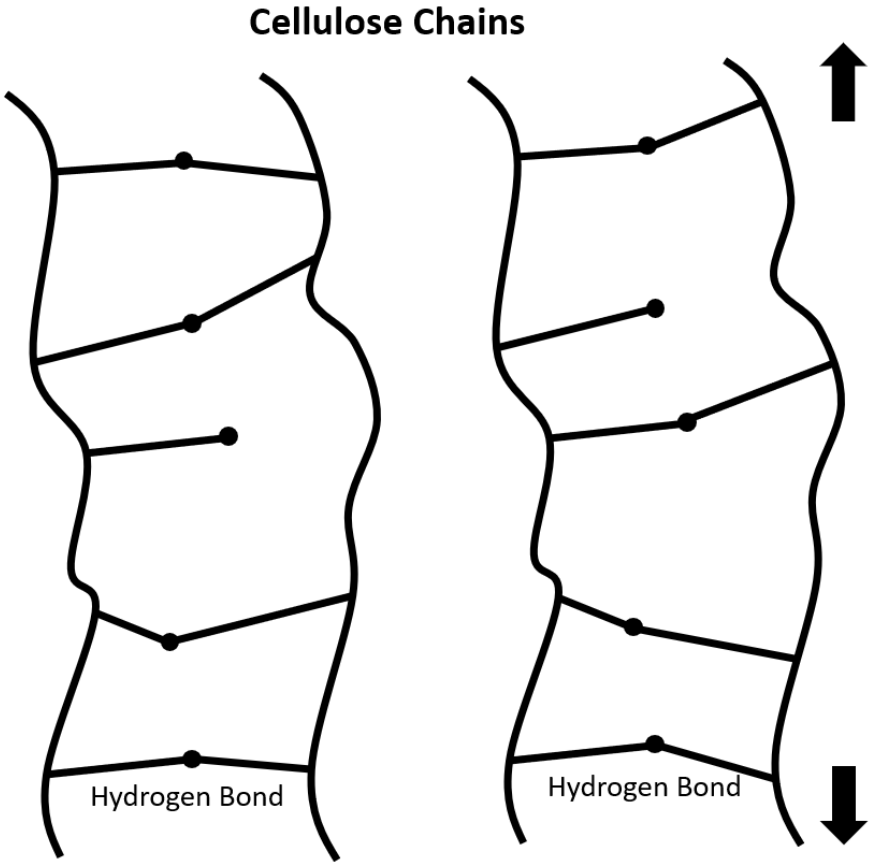

Figure 2.4. Hydrogen bonds breaking and reforming at new sites between cellulose chains in the Grossman model (adapted from Schanzlin 2010).

2.4 Wood Creep Studies

Although the body of research on creep and mechano-sorption in wood and EWPs is significant (Holzer et al. 1989; Morlier 1994), most published data were collected from bending tests on beams (e.g., Toratti 1992) and very few are from tests under compressive loading (Guo 2009; Davies and Fragiacomo 2011; Nguyen et al. 2019).

The difficulty with these studies and the applicability of related models to PT walls considered in this project lays in the fact that the overwhelming majority are concerned with creep under approximately constant loading conditions. When constant loads can be assumed, the sets of constitutive differential equations commonly represented by spring and dashpot diagrams, like that proposed by Fridley et al. (1992), find relatively simple solutions allowing reasonable predictions of the structural behavior of these elements. However, this is not the case for post-tensioned

self-centering shear walls where the PT load and the related tensile deformation of the rods and compressive deformation of the wall are entangled, and neither can be assumed constant. Environmental changes can trigger the mechano-sorptive effect in PT elements as the wood moisture content changes, causing an increase in creep and as a result, a reduction in PT force imposed upon the timber, reducing the creep rate.

Figure 2.5 displays general graphs used to visualize creep (deformation under constant load), relaxation (decline of load when the deformation is constrained), and a mixed case, where neither the load level nor the deformation is constant over time, which is the case for post-tensioned mass timber walls. For post-tensioned mass timber walls, the creep of wood and relaxation of the rods result in a reduction of force and deformation over time. The timber wall creeps due to the compressive force, which reduces the force imposed on the timber wall, and in return, reduces the creep rate.

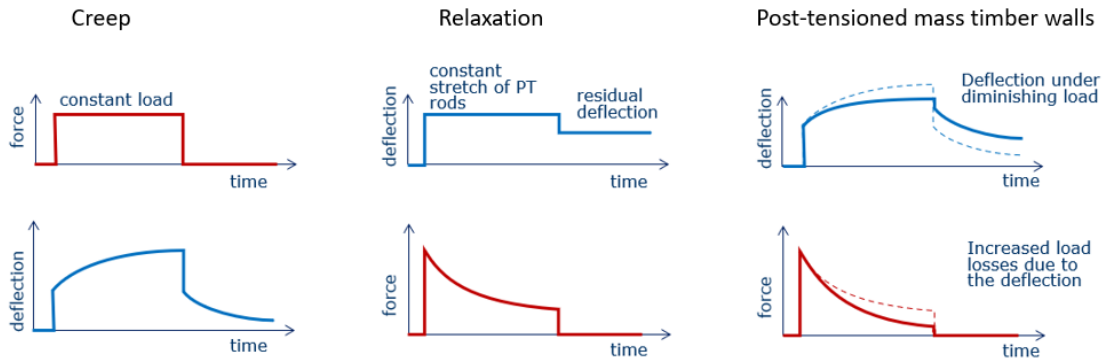

Figure 2.5. Creep, relaxation, and post-tensioned mass timber walls visualized through force and deflection rates (credit: L. Muszynski).

Wood is an orthotropic material which means the material properties vary depending on the direction from which they are measured (Mascia & Lahr 2006). Creep tests in bending are not particularly useful for predicting the creep rate of post-tensioned CLT and MPP panels, where the load is applied in-plane, both parallel and perpendicular to grain, in the different laminations. Timber loaded perpendicular to the grain can reach creep deformations five to eight times higher than when loaded along the grain (Wanniger 2014, Morlier 2004). Only Nguyen et al. (2019) and Grafe

et al. (2018) have tested the in-plane compressive creep behavior of CLT. There are currently no published creep studies on MPP.

Nguyen et al. (2019) attempted to fit a simplified Fridley's model (Fridley et al. 1992) to data obtained from a series of long-term tests on axially loaded CLT panels. PT rods applied compressive stress levels (0.05, 0.10, and 0.15 f'_c) to 3-ply and 5-ply CLT specimens. The specimens were placed in an environmental chamber with a constant temperature and cyclic changes in RH of 50%, 70%, and 90%. Internal moisture gradients resulting from moisture movements within the PT walls volume over 120 days of cyclic exposure were simulated assuming Fick's diffusion model. However, the long-term parameters for Fridley's model could not be identified because the stress levels were diminishing in response to viscoelastic and mechano-sorptive deformations of the PT wall (Nguyen et al. 2019). The authors were also concerned with the adequacy of Fick's diffusion model when applied to CLT panels in which moisture movement is complicated by a crosswise arrangement of layers, each characterized by high transverse anisotropy of moisture conductivity, and inhomogeneities like knots, edge gaps, and adhesive layers. This highlights the need for an alternative modeling approach capable of considering the orthotropic nature of wood and EWPs and, eventually, predicting varying load and deformation conditions in PT shear walls.

2.5 The Material Point Method

The material point method (MPM) is a particle-based method that provides new and demonstrated methods for solving equations for solid mechanics. It has significant advantages over finite element analysis (FEA) when complicated structures, such as composites, are discretized. In MPM, each material point can be assigned different material properties to particles within the same background grid element (Borodin et al. 2005). MPM has potential advantages over FEA in handling multi-physics issues expected to be present in CLT and MPP including the interfaces between layers (Nairn 2018), coupled diffusion of moisture, and cracks that develop in layers or those that exist at non-glued edges in CLT (Nairn 2003). Lastly, many FEA packages often used for modeling viscoelasticity are not readily customizable and transparent

to the user. In contrast, NairnMPM software (2021) is customizable so that innovative modeling solutions can be developed by researchers.

2.6 Structural Health Monitoring

Structural health monitoring (SHM) is generally defined as a damage detection strategy consisting of a network of sensors, a data acquisition system, and algorithms for data analysis (Li 2016). Understanding the structural performance of in-situ timber systems can assist building stakeholders, designers, code officials, and manufacturers through verifying the material performance (Baas et al. 2020b). There is a need to monitor mass timber post-tensioned self-centering shear walls to better understand how the design and maintenance of these systems can be improved and how the contributing factors to PT loss can be mitigated.

2.7 Building Information Modeling

Building information modeling (BIM) is a process for multi-dimensional visualization enabled by a set of software tools and process for facilitating the design, construction, and management of digitally represented physical and functional characteristics of a facility (Teicholz 2013). These models typically contain precise measurements, material data, and information needed to construct the building. The information displayed with a BIM model can depend on what the user is interested in. There are applications for modeling the lifecycle of a building, energy usage, and clash detection used to highlight two building elements modeled in the same location (Eastman et al. 2011).

Not only does BIM provide more possibilities for designing buildings and displaying relevant information, it also can improve communication between stakeholders. Before construction, a BIM may provide the owner with more accurate costs and time (Eastman et al. 2011). Corrections or changes in design can be made and updated to the virtual model in real time. This reduces time wasted waiting during slow communication. The ease of changing one detail presents opportunities for continuous improvement of the design.

A 3D model and construction timeline can be linked together to create a 4D model. An accurate bill of quantities can be generated and used for cost estimation. A 5D model includes the scheduling aspect from a 4D model plus costing. All parties can be aware of the costs associated with a given design.

Building information models are typically developed by an architect or engineer with the purpose of designing a building for construction. The level of detail can vary drastically depending on the objective the BIM is created for. For example, a simple BIM could be created to provide a client options for house renovation projects or a complex BIM could exist for construction managers to plan and coordinate construction processes for a large commercial building. Despite widespread use of BIM during design and construction, they are rarely used to their full capabilities upon the completion of a construction project. Full benefits of BIMs can be realized throughout the lifecycle of facilities as they can be used for SHM, maintenance, storage for cultural and historical documentation, and deconstruction. For these scopes, BIMs can be used to incorporate service life data, such as continuous data from sensors or a routine inspection of built facilities (Boje 2020).

In this study, the use of BIM is explored to correspond SHM data with specific spaces and building elements. Additionally, the BIM model was compared to an as-built model to see if changes were made during construction.

2.8 Digital Twins and Digital Shadows

The digital twin (DT) concept first appeared in the aerospace field and was defined as "a reengineering of structural life prediction and management" (Tuegel 2011). NASA used digital twins for remote monitoring, controlling, and running simulations of their spacecraft from Earth. Next, DTs gained popularity with offshore oil and gas companies to monitor and predict maintenance schedules for their structures for safe and efficient operations. Later, DTs were proposed in manufacturing for efficiency, control, safety, and logistics. Now the use of digital twins is gaining popularity among the built environments. The concept of digital twins is a rapidly growing topic with over 96% of the over 850 academic papers on the topic have been published since 2016. Although fully realized examples are rare, there is a growing amount of

research towards creating digital twins for the built environment. A review by Lamb (2019) breaks down the many research areas of digital twins, with the built environment only providing 5.6% of the studies while manufacturing accounts for almost half.

Digital twins can exist at many scales of complexity, but all should use the best available digital model linked to a data collection network that enables it to accurately represent the physical model (Shafto 2012). Numerous functionalities for DTs include predicting a system's long-term performance, enhancing maintenance communication, and using statistical-based decision making and optimization for building sensors that control systems such as heating and cooling (Macchi 2018).

In this study, the concepts of digital twins and digital shadows are introduced to investigate their potential to help with maintenance decisions due to the increased visualization and details they provide.

3 NUMERICAL MODELING OF IN-PLANE COMPRESSIVE CREEP BEHAVIOR OF CROSS-LAMINATED TIMBER

3.1 Introduction

As post-tensioned systems for LFRS of mass timber buildings gain popularity, there is a need to identify the role of creep resulting in tension loss for post-tensioned timber wall panels. Modeling the creep deformation of post-tensioned mass timber wall panels is important for predicting tension loss to assess if, or when, the tendons should be re-tensioned so their self-centering ability can be restored for seismic resiliency. Creep is a complex phenomenon because as the timber panel creeps, the rods experience PT loss, which affects the creep rate, creating a cycle of changes as time progresses. Accurate creep models must incorporate wood compliance characteristics in major directions and changing moisture profiles to account for the mechano-sorptive effect.

The objective of this study was to create a preliminary material model that reflects the creep rate for mass timber wall panels under a constant load.

3.1.1 Transverse Isotropy

Wood can be roughly considered an orthotropic material, which means the material properties vary depending on the direction from which they are measured (Mascia and Lahr 2006). To accurately model the creep of anisotropic materials, such as wood and mass timber wall panels, creep tests in several axial directions and shear are necessary to predict deformations in a simplified orthotropic case. In terms of engineering elastic models, wood is simplified as orthotropic with different properties associated with three material axes: Longitudinal (L), Radial (R), and Tangential (T) (Mascia and Lahr 2006). For example, timber elements are strongest when the load is applied axially along the grain, also known as the longitudinal direction. Also, physical properties of wood vary in the three anatomical directions. For instance, water diffusivity along the grain is two to three times faster than perpendicular to grain (Siau 1984). Often times, the many different characteristics create difficulties in modeling wood as orthotropic, so wood is simplified as a transversely isotropic

material with one axis of symmetry. Modeling engineered wood products that contain crosswise layers, such as CLT and MPP, is further complicated because the arrangement of panels affects stress distributions, moisture movement, dimension changes, and creep deformations.

3.1.2 Moisture Modeling

To correctly assess the time-dependent response of post-tensioned shear walls, an accurate model of their complex moisture-dependent rheology is needed (Melchor-Placencia and Malaga-Chuquitaype 2021). Fickian models are the most common for moisture transportation. They rely on three main assumptions: 1) the moisture flux is described by a Fickian-type gradient law, 2) the water in the boundary cells is at all times in equilibrium with the surrounding mixture of vapor and air, and 3) the medium is homogenous, which is not true for wood. The most advanced models rely on non-Fickian approaches or multi-Fickian, which requires several material parameters to be defined (Granello and Palermo 2019). In wood, there are two parallel Fickian diffusion processes. There is the diffusion of moisture through the cell wall and the diffusion of water vapor through the air in the system of interconnected cell lumens (Frandsen et al. 2007).

A Python-based code, OpenMoist (Placencia and Malaga-Chuquitaype 2021) has been recently developed to perform one- or two-dimensional transient non-linear moisture diffusion analysis. The code can handle solid and hollow section geometries, moisture dependent parameters and orthotropic diffusion properties typically encountered in wood. The governing differential equations describing the Fickian moisture transfer model in a two-dimensional cartesian coordinate system are used. The model is solved using a time-efficient finite difference algorithm further described by Melchor-Placencia and Malaga-Chuquitaype (2021). This code is convenient because it does not require a software license and allows for customization, which removes research barriers. There is potential for moisture modeling to be incorporated into the creep modeling in a future study so that the moisture content of wood can be calculated at various depths, instead of relying on assumptions based on relative humidity and temperature.

3.1.3 Viscoelasticity

Wood and mass timber wall panels are viscoelastic materials. Viscoelasticity is a theory that allows modeling creep and relaxation behavior of materials and structural elements based on a combination of Hooke's model for elastic solids and Newton's model for viscous liquids. Complex mathematical models reflecting the use of these two elementary models in a variety of combinations are often represented graphically by diagrams in which springs represent Hooke's model of elasticity, and dashpots represent Newton's model of viscous liquids. The springs and dashpots can be connected in parallel, series, or a combination of both.

There are numerous approaches to modeling viscoelasticity of wood. Researchers have developed models to capture the creep behavior of wood-based materials. The power law model, studied by Clouser (1959), Hoyle et al. (1985), and Gerhards (1985) did not include thermal effects on creep. Senft and Suddarth (1971) used a three-element model and Burger model to account for thermal effects on wood creep. Later, Fridley et al. (1992a) used a five-element model to account for mechano-sorptive effects on wood creep behavior. The coincident element method was used to model examples of viscoelasticity of laminated composites but was restricted to shell problems (Nallainathan et al. 2004; Martynenko 2017). A differential approach was used by combining dashpots and springs in viscoelastic models for timber structures (Vidal-Salle and Chassagne 2007; Fortino et al. 2009; Huc and Svensson 2018). In a study by Vidal-Salle and Chassagne (2007), the viscosities of two Maxwell elements depend on the stress level and moisture changes. None of the studies investigated the effect of time-dependent Poisson's ratios on creep behavior. Bengtsson et al. (2020) examined the 3D creep of wood and composite materials and summarized the progression of viscoelastic models. Bengtsson et al. (2020) found that applying time-dependent Poisson's ratios to the model gave similar results to experimental data. This study also found that two exponential terms may be used based on available experimental data and if necessary, a constant Poisson's ratio can be used if it has been shown that the Poisson's ratios are time-independent in the experimental testing.

3.2 3D Anisotropic Viscoelasticity Modeling Method

While finite element software packages like ABAQUS are often used for modeling viscoelasticity, some element definition codes in these packages are not readily open to the user and do not allow necessary customization. Therefore, a material point method (MPM) code engine developed by Dr. John Nairn, OSParticulas (2021) was selected as an alternative approach.

Preliminary modeling was performed by implementing 3D, anisotropic viscoelasticity, including a novel approach to modeling mechano-sorptive effects, into custom material point method (MPM) software called OSParticulas (Nairn 2021). The MPM is a particle-based, computational mechanics method that discretizes the object into material points on a background calculational grid (Sulsky et al. 1994). It numerically solves the same equations as finite element analysis (FEA), but by a different approach. MPM has potential advantages over FEA in handling multi-physics issues expected to be present in CLT and MPP including interfaces between layers (Nairn 2018), coupled diffusion of moisture, and cracks that develop in layers or those that exist at non-glued edges in CLT (Nairn 2003). More details on MPM calculations can be found elsewhere (Nairn and Bardenhagen and Smith 2018; Nairn and Hammerquist 2021).

In the material point method, isotropic materials have a separate constitutive law to enhance efficiency by ignoring terms that only apply to anisotropic materials. For wood, the 3D stiffness equations in the material axis system are shown in Eq. 3.1 where $\varepsilon_{ii}^{(res)}$ are residual strains in the normal directions (Nairn 2021).

$$\begin{pmatrix}\sigma_{xx}\\ \sigma_{yy}\\ \sigma_{zz}\\ \tau_{xz}\\ \tau_{yz}\\ \tau_{xy}\end{pmatrix} = \begin{pmatrix}C_{11} & C_{12} & C_{13} & 0 & 0 & 0\\ C_{12} & C_{22} & C_{23} & 0 & 0 & 0\\ C_{13} & C_{23} & C_{33} & 0 & 0 & 0\\ 0 & 0 & 0 & C_{44} & 0 & 0\\ 0 & 0 & 0 & 0 & C_{55} & 0\\ 0 & 0 & 0 & 0 & 0 & C_{66}\end{pmatrix} \begin{pmatrix}\varepsilon_{xx} - \varepsilon_{xx}^{(res)}\\ \varepsilon_{yy} - \varepsilon_{yy}^{(res)}\\ \varepsilon_{zz} - \varepsilon_{zz}^{(res)}\\ \gamma_{xz}\\ \gamma_{yz}\\ \gamma_{xy}\end{pmatrix} \tag{3.1}$$

Modeling creep and mechano-sorption in computational mechanics requires methods for 3D, anisotropic viscoelasticity. One-dimensional modeling of linear viscoelastic materials can be extended to 3D using a tensor form of the Boltzman superposition integral:

$$\boldsymbol{\sigma}(t) = \int_0^t \mathbf{C}(t-u)\frac{\varepsilon(u)}{du}du \tag{3.2}$$

where $\boldsymbol{\sigma}$(t) is a time-dependent stress tensor, $\boldsymbol{\varepsilon}$(u) is the strain tensor, and **C**(t) denotes a fourth-ranked, time-dependent stiffness tensor (Bengston et al. 2020). Wood is commonly treated as an orthotropic material which would result in **C**(t) potentially having nine time-dependent characteristics. The experiments to determine all these properties for wood are not available. To reduce the number of needed properties, wood was simplified as a transversely isotropic material with five independent properties. If the 1 direction is the longitudinal direction of wood with 2 and 3 being the transverse directions, the five needed properties are $C_{11}(t) = n(t) = E_A(t) + 4K_T(t)\nu_A(t)^2$, $C_{12}(t) = C_{13}(t) = l(t) = 2K_T(t)\nu_A(t)$, $C_{22}(t) = C_{33}(t) = K_T(t)+G_T(t)$, $C_{23}(t) = K_T(t)-G_T(t)$, $C_{44}(t) = G_T(t)$, and $C_{55}(t) = C_{66}(t) = G_A(t)$, where **C**(t) denotes a fourth-ranked, time-dependent stiffness tensor represented as a 6X6 matrix in Voight notation (Eq. 3.3). Here E_A is the axial modulus, K_T is the plane strain bulk modulus, G_A and $G_T=E_T/(2(1+\nu_T))$ are the axial and transverse shear moduli, n and ℓ give time-dependence of the C_{33} and $C_{13}=C_{23}$ elements of the stiffness tensor (Nairn et al. 2018). E_T is the transverse modulus, ν_A is the axial Poisson's ratio, and ν_T is the transverse Poisson's ratio (Nairn et al. 2018).

$$\mathbf{C} = \begin{bmatrix} K_T+G_T & K_T-G_T & \ell & 0 & 0 & 0 \\ K_T-G_T & K_T+G_T & \ell & 0 & 0 & 0 \\ \ell & \ell & n & 0 & 0 & 0 \\ 0 & 0 & 0 & G_A & 0 & 0 \\ 0 & 0 & 0 & 0 & G_A & 0 \\ 0 & 0 & 0 & 0 & 0 & G_T \end{bmatrix} \tag{3.3}$$

The goal was to derive a reasonable set of viscoelastic properties consistent with available experiments on wood, such as longitudinal and transverse creep experiments by Hu and Guan (2018). A common practice for isotropic materials is to reduce to a single time-dependent shear modulus while assuming the bulk modulus is independent of time. That approach does not work for anisotropic materials because allowing only shear moduli to depend on time predicts the material will never creep in the longitudinal direction, which is not true for axially loaded post-tensioned timber walls. To handle observed creep in all directions, all five elements of **C**(t) were allowed to follow a sum of relaxation times:

$$M(t) = M_0 + M_1 e^{-t/\tau_M} \tag{3.4}$$

where M(t) is a sum of exponentials where M_0 is the relaxed or long-term modulus, $M_e = M_0+M_1$ is the instantaneous or elastic modulus, and τ_M is the single relaxation time for property M. One lifetime was used unless more were needed. Each property is expanded in terms of exponential decay functions in equations 3.5 through 3.9.

$$n(t) = n_0 + \sum_{k=1}^{N_n} n_k e^{-t/\tau_{n,k}} \tag{3.5}$$

$$K_T(t) = K_{T0} + \sum_{k=1}^{N_{KT}} K_{Tk} e^{-t/\tau_{KT,k}} \tag{3.6}$$

$$G_A(t) = G_{A0} + \sum_{k=1}^{N_{GA}} G_{Ak} e^{-t/\tau_{GA,k}} \tag{3.7}$$

$$\ell(t) = \ell_0 + \sum_{k=1}^{N_l} \ell_k e^{-t/\tau_{\ell,k}} \tag{3.8}$$

$$G_T(t) = G_{T0} + \sum_{k=1}^{N_{GT}} G_{Tk} e^{-t/\tau_{GT,k}} \tag{3.9}$$

The first calculations revealed the properties are not entirely independent with some choices leading to thermodynamically impossible negative creep. To solve this issue, relaxation times for K_T and ν_A were made the same and it was determined that valid properties required ν_A to increase with time such that:

$$\nu_{A0} \geq \left(1 + \frac{K_{T1}}{2K_{T0}}\right)\nu_{Ae} \tag{3.10}$$

The derivation includes differentiation of modulus and rearranging of equations that requires Eq. 3.10 be met.

First, the longitudinal experiments were fit by using a single relaxation time, $\tau_{M,}$ for $K_T(t)$ and $\nu_A(t)$ and varying the coefficients K_{T0}, K_{T1}, ν_{A0}, and ν_{A1}. It was determined that fitting experimental results required using two relaxation times for $C_{11}(t) = n(t)$. Next, the transverse direction was fit using a single relaxation time GT(t) and varying only G_{T0}, G_{T1}, and τ_{GT} (the properties for $G_A(t)$ did not affect these 2D calculations). Experimental results from Hu and Guan (2018) showed small differences between radial and tangential creep, but refined modeling to capture such differences would require extension to orthotropic materials with nine time-dependent

terms. This modeling based on transversely isotropic materials can only examine the much larger differences between axial and transverse experiments.

In some viscoelasticity results, creep compliance is reported rather than strain. Creep compliance is defined by strain variations under constant unit stress (Ikegami 2001). For a creep test at constant stress, the creep compliance is:

$$J(t) = \frac{e(t)}{s} \tag{3.11}$$

where *J(t)* is creep compliance, *e(t)* is total strain, and *s* is a constant stress. The creep strain reported by Hu and Guan (2018) was mathematically rearranged so values from the model could accurately be compared. Hu and Guan (2018) displayed their results of creep strain after subtracting the initial strain. In other words, they report $(C_t\text{-}C_0)/L$ where initial strain, C_0/L, is subtracted from total strain C_t. Their reported relative creep results (denoted here by *ecr*) can be converted to creep compliance by:

$$J(t) = \frac{(\frac{C_0}{L} + ecr)}{s} = \frac{(\frac{s}{E} + ecr)}{s} = (\frac{1}{E})(1 + \frac{E * ecr}{s}) \tag{3.12}$$

Next, Equation 3.12 can be expressed as relative result by using creep compliance multiplied by the modulus:

$$J(t) * E = (1 + \frac{E * ecr}{s}) \tag{3.13}$$

Equation 3.13 provides a notation used to make comparisons between the results by Hu and Guan (2018) and the results from the material model.

3.3 Results

The MPM simulations modeled a 20 mm long specimen (axial direction) that was 5 mm wide using a background grid with 0.833 x 0.833 mm cells. By symmetry, the model included only half the specimen in the width direction (2.5 mm) leaving 6 cells

in the width. Each cell had 4 materials points or 12 material points in the specimen width (0.417 mm x 0.417 mm particles). This resolution was verified as sufficient for these constant-stress and uniaxial conditions. To avoid dynamic effects caused by applying a constant stress, the desired stress was ramped to the final value using a sigmoidal ramp and then held constant. Simulation output for axial strain was converted to J(t)*E(0) results. The best-fit modeling results in Figure 3.1 are compared to the published longitudinal creep test and an average of the radial and tangential experiments (Hu and Guan 2018). The plots are for creep compliance (J(t)) times initial modulus (E(0)) in each direction to allow visualization of both longitudinal and transverse results on the same scale. The two directions could be fit well. The fitting parameters, however, are not unique. Many more viscoelasticity experiments are needed to refine all the possible time-dependent parameters (*e.g.*, experiments in shear, biaxial stress, and transverse compression). The properties used for these fits in Table 3.1 output the material properties shown in Figure 3.2.

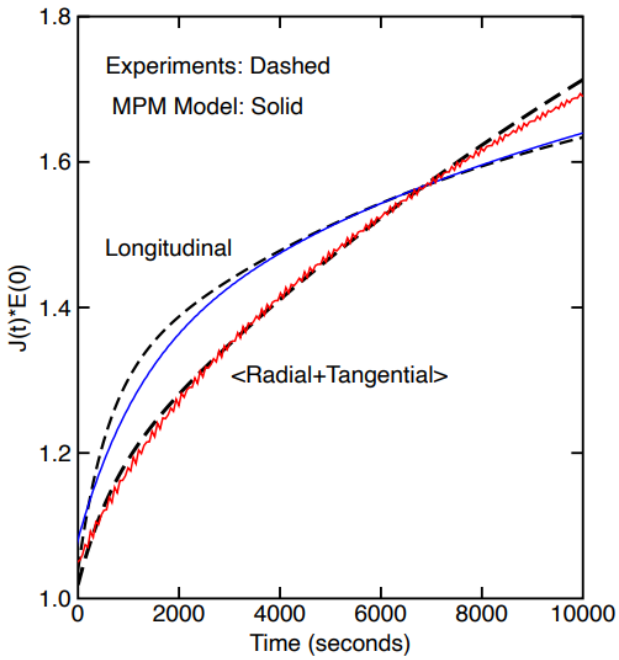

Figure 3.1. The MPM model (solid) fitted to the experiments of Hu and Guan (dashed).

Table 3-1: Chosen elastic wood properties as a transversely isotropic material displayed in OSParticulas

Elastic Wood Properties as a Transversely Isotropic Material						
E_A	G_A	v_T	v_A	E_T	G_T	rho
10,000	625	0.7	0.5	500	147	0.00055

```
Material 1: TI Viscoelastic 1 Material
     Tranversely isotropic viscoelastic (unrotated A axis along z axis) with:
EA  = 10000         ET  = 500           vA  = 0.5           vT  = 0.7
GT  = 147.059       GA  = 625           vA' = 0.025         KT  = 909.091
n   = 10909.1       ell = 909.091       K   = 909.091
GT0 = 73.5294       ntaus= 1
  i = 1             GTk = 73.5294       tauk= 0.3 ms
GA0 = 312.5         ntaus= 1
  i = 1             GAk = 312.5         tauk= 0.3 ms
KT0 = 454.545       ntaus= 1
  i = 1             KTk = 454.545       tauk= 0.3 ms
n0  = 6545.45       ntaus= 2
  i = 1             nk  = 2181.82       tauk= 4 ms
  i = 2             nk  = 2181.82       tauk= 0.4 ms
ell0= 727.273       ntaus= 1
  i = 1             ellk= 181.818       tauk= 0.3 ms
Isothermal and isosolvent viscoelasticity
aA  = 5             aT  = 40
Large rotation method for hypoelastic materials
rho = 0.00055
Crack Growth Criterion: No propagation
```

Figure 3.2. Output file from OSParticulas showing the material properties for wood as an isotropic material

3.3.1 Proposal for Modeling Mechano-sorption

Shift-factor methods, common in modeling temperature effects, were used for viscoelasticity to model mechano-sorption in 3D computational mechanics. These methods assume temperature and moisture change only relaxation times (τ_M) while having no effect on modulus coefficients (M_0 and M_i). A general shift factor approach recasts Eq. 3.2 using an *effective* time defined by:

$$t_{eff} = \int \frac{dt}{a_{\text{total}}} \tag{3.14}$$

where $a_{total} = a_T\, a_m\, a_{ms}$ is the product of shift factors relating to temperature, moisture, and mechano-sorption. a_T and a_m (to a lesser extent) are standard superposition methods used in linear viscoelasticity modeling. The addition of a_{ms} is a new approach to mechano-sorption that reimagines it as part of a material's viscoelastic relaxations rather than a separate mechanical mechanism seen only in wood. The mechano-sorptive effect is triggered by adsorption or desorption (Fridley et al. 1992), so the magnitude of a_{ms} is related to the absolute value of the moisture change rate to model effects seen during both increasing and decreasing moisture content.

3.4 Conclusions, Limitations, and Future Work

The Material Point Method was used to simulate the creep deformation of wood as a transversely isotropic material. The material properties were chosen based on the results from the creep tests conducted by Hu and Guan (2018). The longitudinal and transverse directions fit well, but many more viscoelasticity experiments are needed to refine all the possible time-dependent parameters. A new approach to modeling mechano-sorptive creep was proposed. The shift-factor method reimagines mechano-sorption as part of a material's viscoelastic relaxations rather than a separate mechanical mechanism seen only in wood.

A limitation of this study includes the constant force applied to the wood in the longitudinal direction. This cannot be transposed to predict the creep of EWPs within a post-tensioned structural system due to the loss of tensile force in the steel rods. Additionally, the shift-factor method for modeling mechano-sorptive creep was not tested due to a limitation of data in literature required to calibrate the model. Other limitations with the model exist due to the cross-wise layers of CLT and MPP. To clarify, stress is distributed differently among each ply due to the product's heterogenous layup and orthotropic nature. Lastly, the effects of glue bond lines were disregarded in this model. Glue lines between plies affect stress distribution and

moisture diffusion across plies. Future work can include incorporating the effects of glue bond lines to represent the mass timber panels more accurately.

This model provides the preliminary steps toward modeling PT loss for CLT and MPP walls exposed to a variable environment. The material model can be updated to provide more accurate creep parameters and PT loss predictions for CLT and MPP elements based on the data collected from the proposed creep tests discussed in Chapter 4. This simulation will be useful for the design of self-centering shear walls, construction practice of tensioning rods, and maintenance of these systems. Predictive capabilities have the potential to inform building managers of tension loss through structural monitoring data paired with models to act as a digital twin (Longman et al. 2021).

4 POST-TENSIONED SELF-CENTERING CROSS-LAMINATED TIMBER AND MASS PLYWOOD PANELS CREEP TEST DESIGNS AND METHODOLOGIES

Overview

The following sections propose methodologies for axially loaded CLT and MPP creep tests in a constant environment, varying environment, and as a full-scale structural system in an uncontrolled indoor environment. The methodologies focus on measuring deformations and the load imposed on the timber walls by post-tensioned rods from a material scale to a structural system. In a future study, the data from these tests can refine the material model to predict the PT loss of post-tensioned timber walls and validate the model against SHM data obtained from real examples (Figure 1.1).

4.1 Introduction

Post-tensioned timber walls experience PT loss over time, negatively affecting their seismic resiliency. Viscoelastic creep and mechano-sorptive creep largely impact the PT loss of these structural systems. However, the creep rate of CLT and MPP are not well known. These material parameters must be studied to inform a material model so recommendations to the design and maintenance of PT systems can be made. Small-scale tests are designed to capture the material properties of mass timber walls. Full-scale post-tensioned timber walls are designed to examine creep and PT loss. Together, these studies can refine material models to create a model that predicts the creep and PT loss of mass timber wall panels.

The objectives of this study are to:

1) Develop a methodology that outlines the specific steps and requirements to measure the in-plane creep of CLT and MPP.

2) Develop a methodology for monitoring full-scale post-tensioned CLT and MPP wall panels.

4.2 Materials and Methods

The next sections include detailed methodologies for:

1) Small-scale creep tests on CLT and MPP to identify material parameters used to predict in-plane viscoelastic and mechano-sorptive creep, to refine material models, and
2) Long-term full-scale tests to analyze the entangled effects of creep and tension loss in an uncontrolled and realistic environment.

4.3 Small-scale Creep Test Methodologies

Small-scale tests were designed to gather material-specific data regarding creep. The data generated from a constant environment creep test is subtracted from the strain data from specimens placed in a varying environment, to separate the mechano-sorptive effect. Unloaded specimens, designed to experience no creep deformations, are subjected to the same varying environment to record the shrinkage and swelling effects due to a fluctuating moisture content. These known deformations are needed to separate creep deformations from the shrinkage and swelling deformations. Figure 4.1 displays the small-scale tests with their differences in environmental conditions and loading needed to separate the mechano-sorptive creep, viscoelastic creep, and shrinkage and swelling parameters of CLT and MPP.

The test procedures generally follow the methodology outlined by Muszynski et al. (2005) which allow comprehensive separation of the viscoelastic and mechano-sorptive components of the deformations recorded in varying climate conditions, as well as the moisture-induced dimensional changes (shrinkage and swelling). Before testing, the specimens are placed in a constant environment to reach a known EMC.

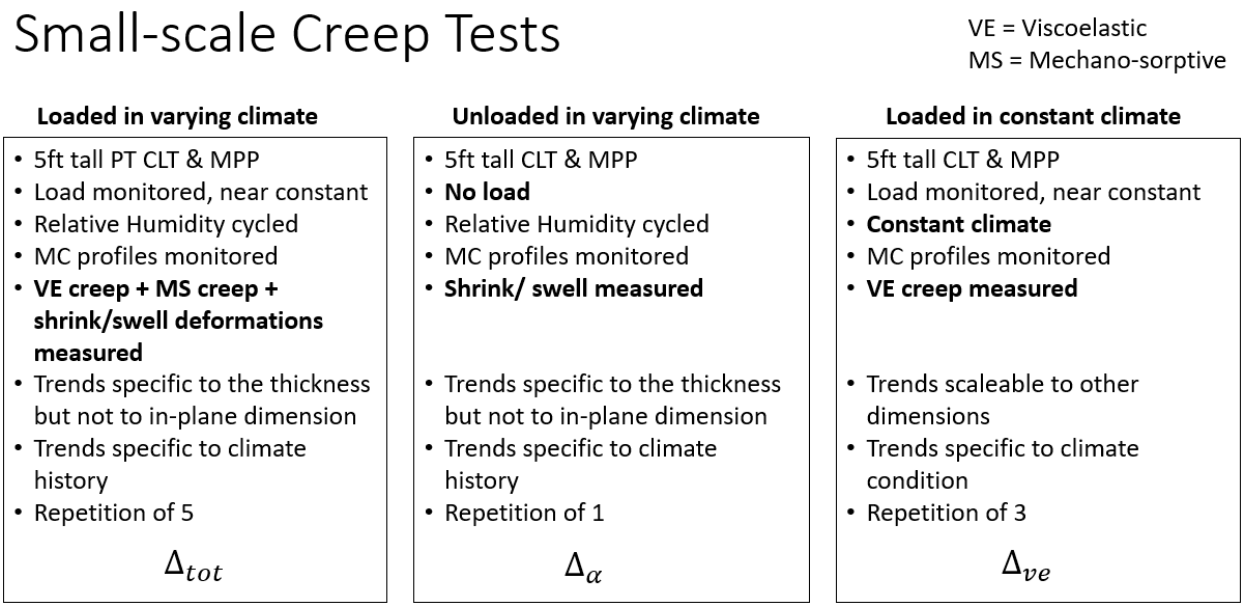

Figure 4.1. Small-scale creep tests listed with measurands including loading conditions, environment, and creep deformations

4.3.1 Constant Environment Creep Test

The constant environment creep tests are performed to estimate the viscoelastic creep characteristics of the panels. A constant environment at 65% RH and 30 ºC is chosen. The proposed duration of the test is 52 weeks so long-term data on the second stage of creep are recorded. Creep characteristics determined in the constant environment are used to estimate the viscoelastic component of the total panel deformation recorded under the variable environment and separate the mechano-sorptive effect experienced in the varying environment creep test.

4.3.2 Varying Environment Creep Test

The varying environment creep tests are performed on five CLT specimens and five MPP specimens placed in an environmental chamber. The chamber subjects specimens to six relative humidity cycles between 30% and 90% with a constant temperature of 30 ºC (equivalent to 6% and 20% equilibrium MC in wood) (Forest Products Laboratory, 2010). The diffusion of moisture is observed during each cycle lasting 2 weeks with a total test duration of 12 weeks. The diffusion of moisture

through 5-ply CLT and 6-inch MPP is slow, so specimens are expected to experience a delayed moisture content response to the varying relative humidity.

Changes in moisture gradient profiles through the thickness of the test specimens at the end of each cycle are determined by slices from small, sacrificial CLT and MPP blocks placed in the chamber. Each slice is cut into small sections to represent different depths and the moisture content at each depth is determined based on the oven dry method (ASTM D4442-20 2020). The moisture content profiles are used to validate the simulation of moisture diffusion through the test panels.

An unloaded CLT and MPP specimen is placed in the same environment and instrumented with LVDTs to record the free shrinkage and swelling effects due to the fluctuating timber moisture content. These specimens will not creep because there is no load, but they are important for extracting the shrinkage and swelling effects from the data so the creep rate is revealed.

The mechano-sorptive creep is extracted by subtracting the constant environment creep test data from the varying environment creep test data. In the end, viscoelastic creep, mechano-sorptive creep, and shrinkage and swelling effects are separated. The tests should allow a reliable definition of the time- and moisture-dependent stiffness matrix for the constitutive model for wood. In a future study, these parameters can be used to refine the material model to predict the creep of CLT and MPP exposed to ambient climate conditions.

4.3.3 Small-scale Specimen Designs

The small-scale CLT and MPP specimens are edge-sealed to force unidirectional moisture transfer through the faces. Wood filler is first applied to the edges to fill any holes or gaps in the wood before applying a waterproof, elastomeric seal to prevent moisture diffusion while keeping the wood unrestrained to allow for dimensional changes. The PT action is simulated by two external threaded steel rods with a 12.7 mm (0.5 in) diameter placed parallel with the major direction of the panel. The load is transferred through two steel anchorage plates. Four rail car springs are welded between the bottom anchor plates to reduce the effect of relaxation of the post-tensioned rods due to the creep deformation of the wood. This design helps maintain

a constant PT force equivalent to 0.1 f'_c (where f'_c is the gross section adjusted allowable compressive stress of the panels). The springs are arranged in groups of four, based on their stiffness. The PT force is monitored throughout the test by load cells positioned on levelling washers, while deformations are measured using LVDTs. Each specimen is instrumented with two load cells, one per rod, and one LVDT placed along the height of the panel, located in the middle of the panel.

The tensioning procedure is devised taking spatial restrictions of the environmental chamber into consideration. In this case, manually tensioning each rod with a torque wrench and multiplier proved to be an exhaustive, yet sufficient option. It is advised to tension each rod in 1,000 lb. increments to reduce the effects of uneven loading, such as local crushing, until the desired PT force is reached.

4.3.4 Small-scale Cross-laminated Timber Specimens

The CLT specimens are Douglas-fir (*Pseudotsuga menziesii*) 5-ply CLT (grade V1 – ANSI/APA PRG 320-2019) specimens representing the type of material used in the first and currently only CLT post-tensioned structure built in the United States. Dimensions of each panel are 1.52 m x .457 m x .174 m (60 in. x 18 in. x 6.8 in). The height of the panel is maximized so the creep deformation will be larger and easier to measure, but the height is constrained based on the size of the environmental chamber. The width of the panel was chosen to create similar proportions to the wall panels in Peavy Hall, while the thickness corresponds to 5-ply CLT. Drawings of the specimen design that include the CLT panel, threaded rods, and steel plates used for tensioning are shown in Figures 4.2 and 4.3. The top plate includes two holes for the external tensioned rods distanced to account for the thickness of the 5-ply CLT and to avoid direct contact of the tensioned rods with the faces of the panel (Figure 4.4). Figure 4.5 shows a CLT specimen prototype used to test the post-tensioning procedure.

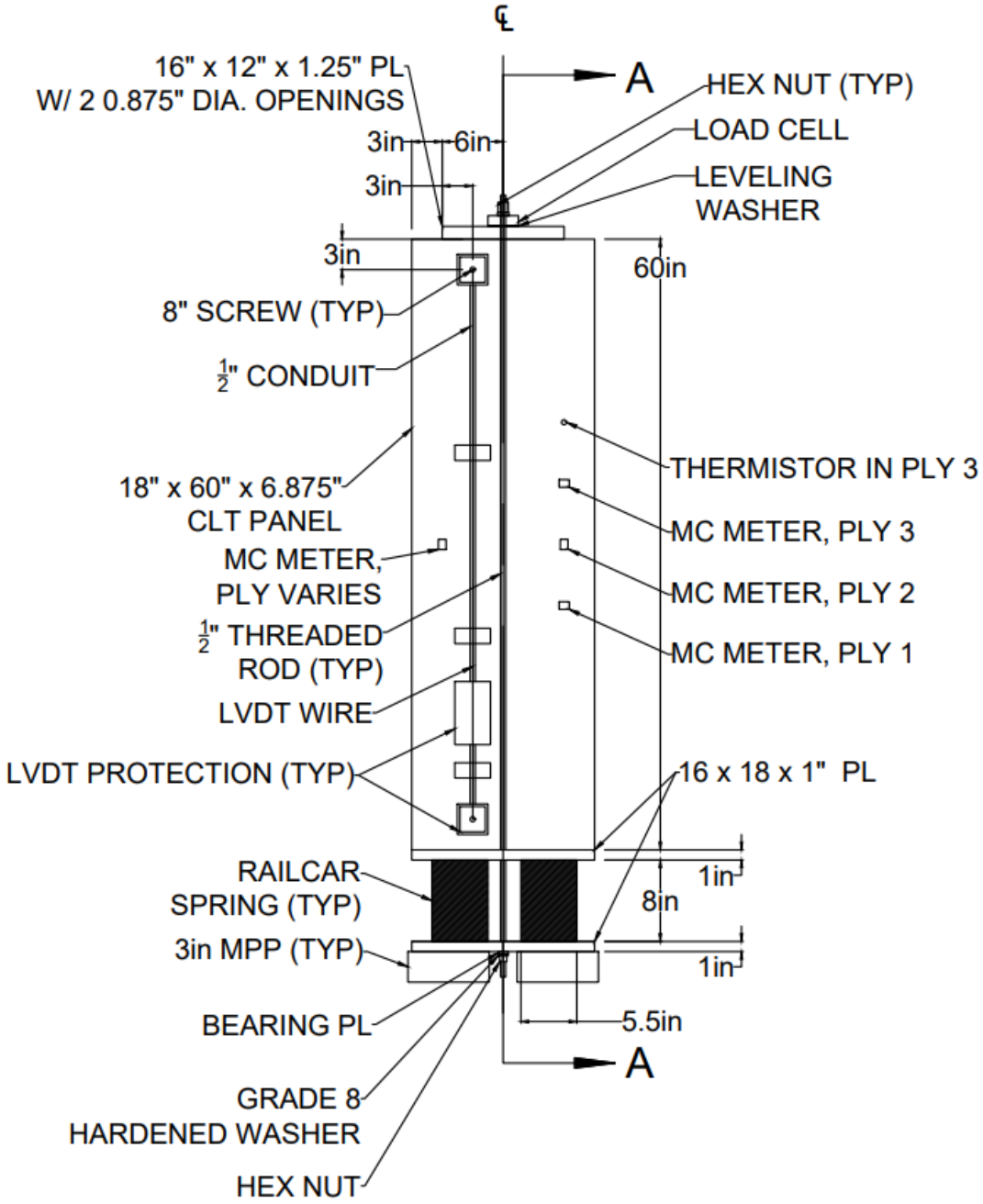

Figure 4.2. Elevation view of the small-scale CLT specimen design (credit: E. Baas)

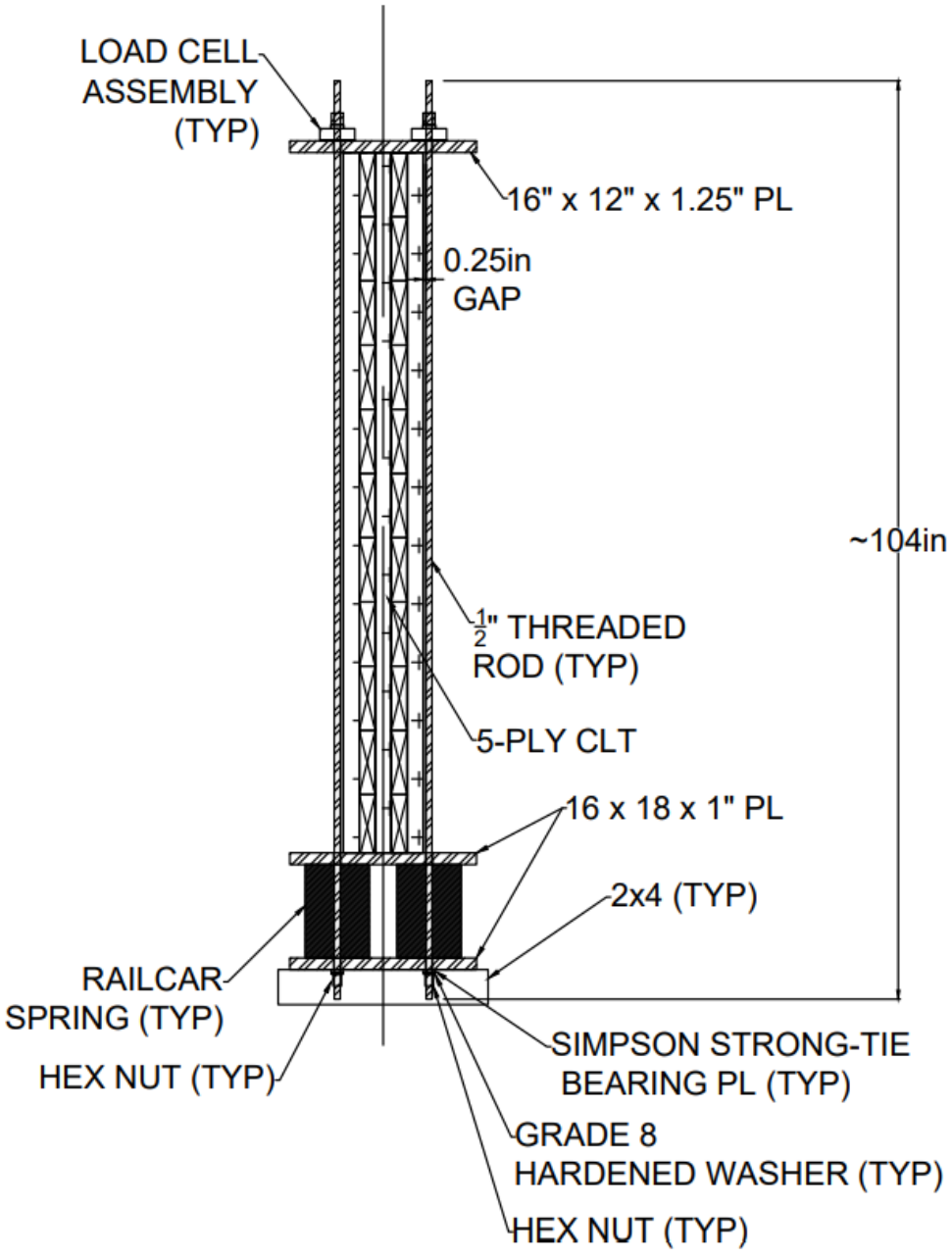

Figure 4.3. Section view of the small-scale CLT specimen design (credit: E. Baas)

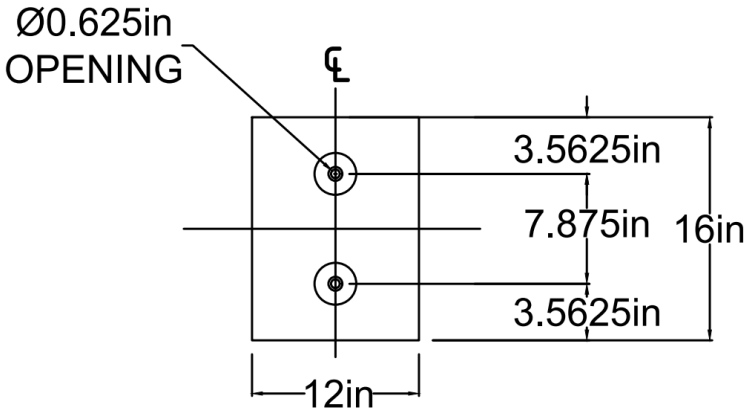

Figure 4.4. Plan view of small-scale CLT specimens (credit: E. Baas)

Figure 4.5. Small-scale CLT specimen attached to a crane as a safety precaution.

4.3.5 Small-scale Mass Plywood Panel Specimens

The MPP specimens are Douglas-fir (*Pseudotsuga menziesii*) 6-inch thick MPP specimens with dimensions of 1.52 m x .457 m x .152 m (60 in. x 18 in. x 6 in). Once again, the height was maximized based on the dimensions of the environmental chamber, the width matched the proportion of the panel to mass timber walls, and the thickness corresponds to 6-inch MPP. Drawings of the specimen design that include the MPP panel, threaded rods, and steel plates used for tensioning are shown in Figure 4.6 and Figure 4.7. The top plate includes two holes for the external tensioned rods distanced apart to account for the thickness of the 6-inch MPP plus an air gap, so the tensioned rods do not contact the faces of the panel (Figure 4.8).

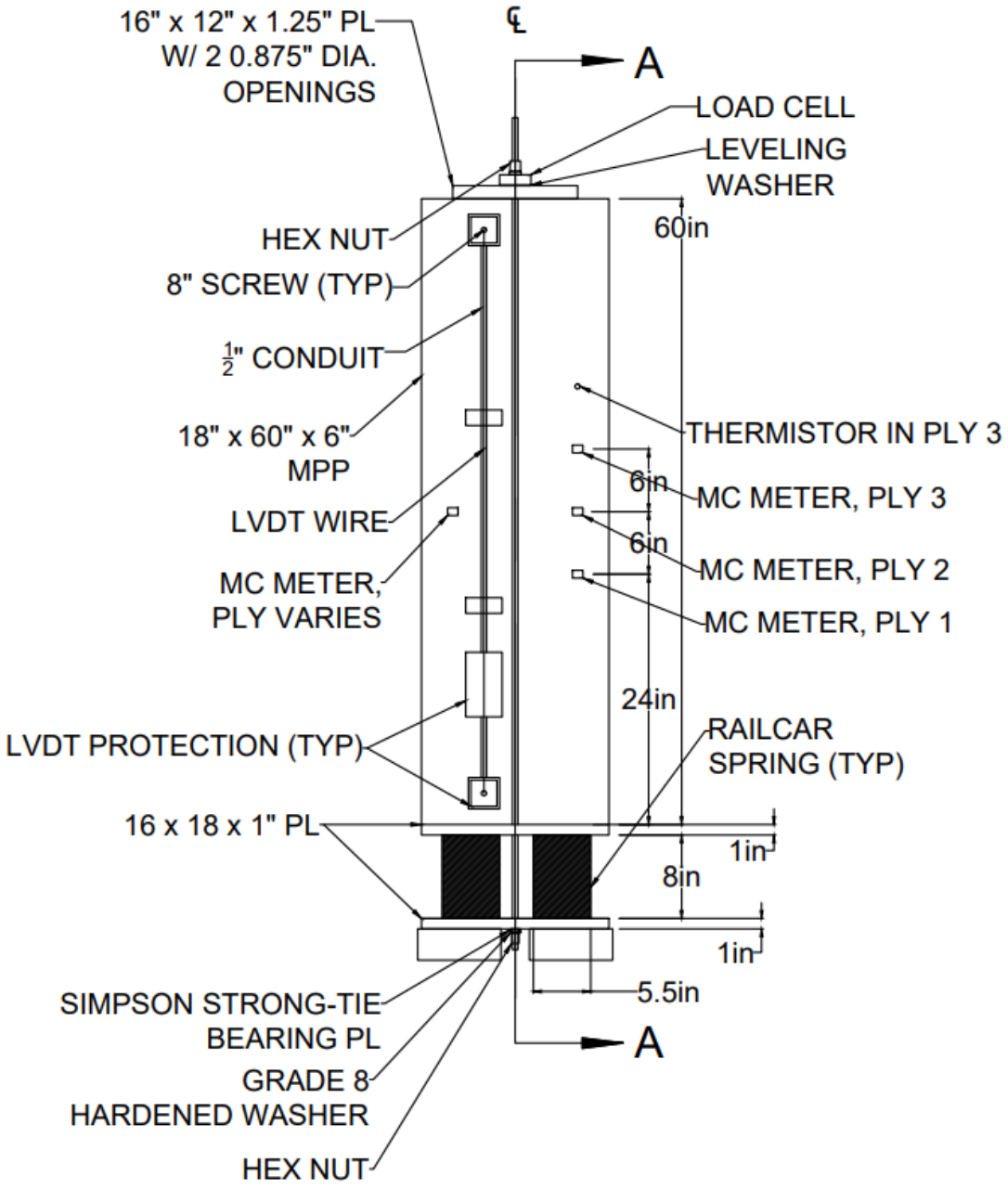

Figure 4.6. Elevation view of the small-scale MPP specimen design (credit: E. Baas).

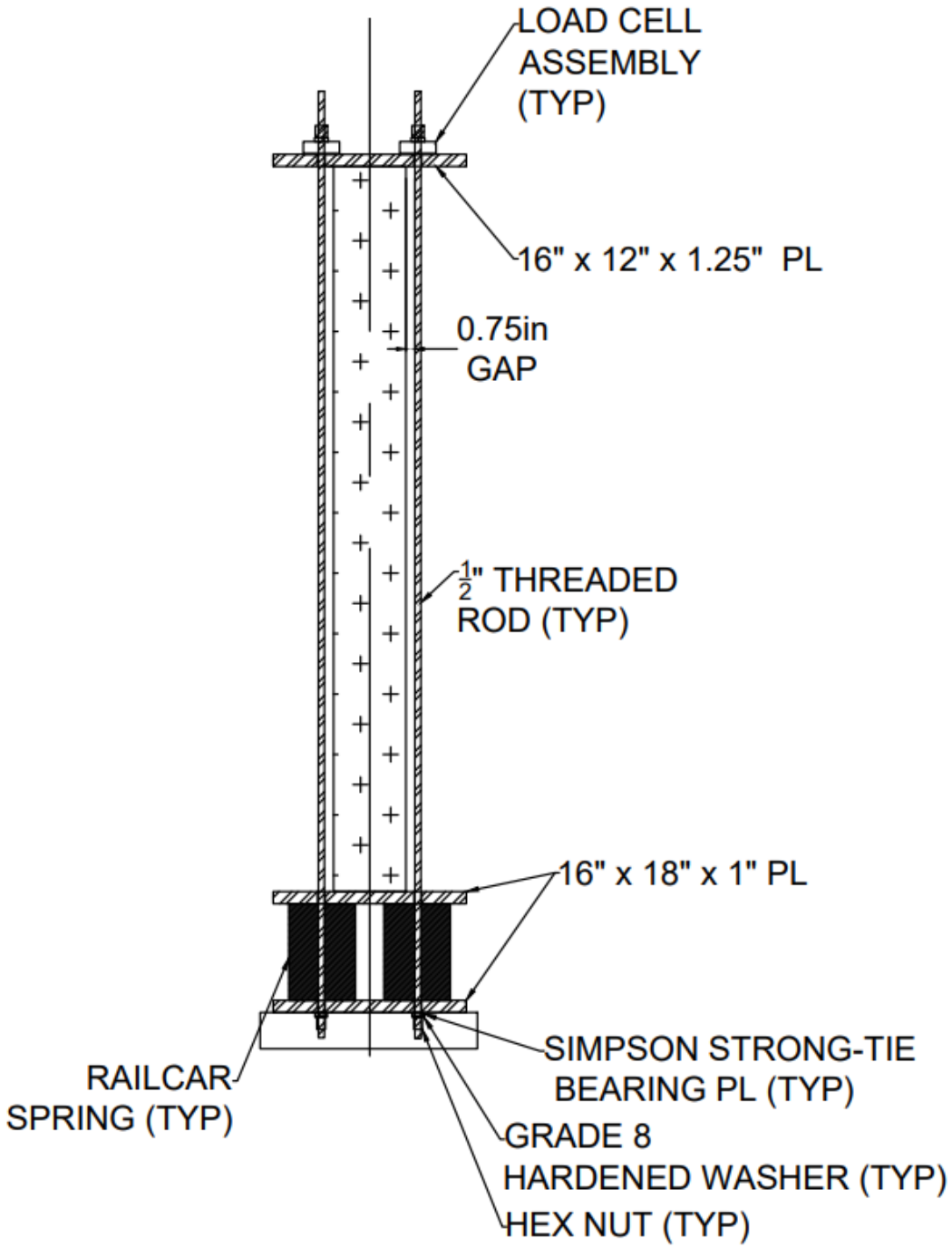

Figure 4.7. Section view of the small-scale MPP specimen design (credit: E. Baas)

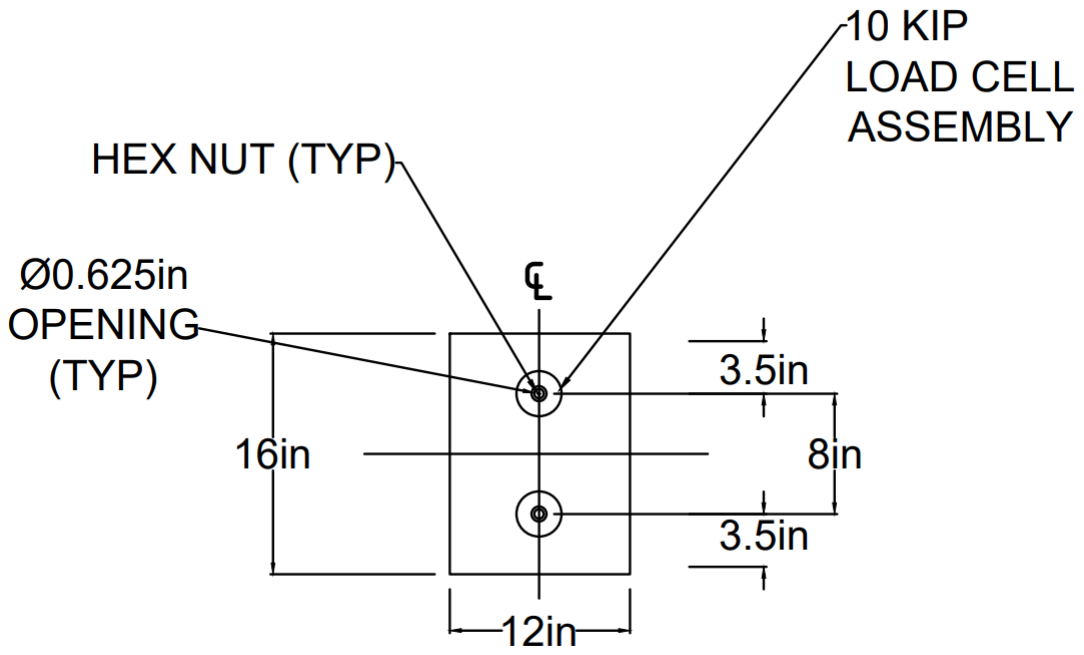

Figure 4.8. Plan view of small-scale MPP specimens (credit: E. Baas)

4.4 Methodology for Monitoring Full-scale Post-tensioned Timber Walls

This section describes the experimental design to monitor creep and post-tension losses of full-scale CLT and MPP post-tensioned walls in an indoor uncontrolled environment (Figure 4.9). The test location is the A.A. “Red” Emmerson Lab at Oregon State University.

A methodology for monitoring full-scale post-tensioned CLT and MPP walls is presented. These walls are used to analyze the role of creep in PT loss. The material model created from the small-scale creep tests can be updated to include PT loss, in the form of a varying load. The model can be validated against the data collected from an actual CLT post-tensioned building, where the walls are connected to other building elements.

In addition to assessing the long-term performance of these systems, the experiment aims to evaluate local phenomena occurring during post-tensioning, such as local crushing of the panel under the top plates, which may cause immediate tension loss. For this purpose, a full-field optical measurement system based on the

digital image correlation (DIC) method is used to measure the strain of each panel during tensioning, with a focus on the top section of the panel. Additionally, another optical measurement unit placed on the opposite side of the laboratory measures the strain distribution, and total wall deformation due to creep and moisture changes. To obtain accurate DIC measurements, each wall is painted with a speckle pattern and paper targets are added to the face of each wall in a grid pattern.

Additionally, each wall is instrumented with two LVDTs, placed on the panel faces, to measure the total deformation of the wall. Another LVDT is positioned transversally on the panel edge to measure out-of-plane deformations. Therefore, total deformations, including creep, mechano-sorptive creep, and shrinkage and swelling, are measured by combining local, contact measurements with LVDTs and global, optical measurement with DIC. Each rod is instrumented with a load cell, with a through-hole for the rod, to measure PT loss.

The temperature and relative humidity of the environment is recorded with sensors in the laboratory. These data are used to evaluate effects of environmental fluctuations on the test. However, they are not sufficient to accurately derive the moisture content of the walls, and especially moisture gradients within each panel. The average moisture content in the panels is estimated with periodic, local readings using both resistance and capacitance moisture meters at different locations. For more accurate results, every two weeks, sacrificial CLT and MPP elements near the walls are sliced into strips and cut at various depths and oven-dried to directly determine a moisture content profile. A test duration minimum of 52 weeks is specified to observe the second stage of creep and analyze the long-term entangled effects of creep and tension loss in an uncontrolled environment.

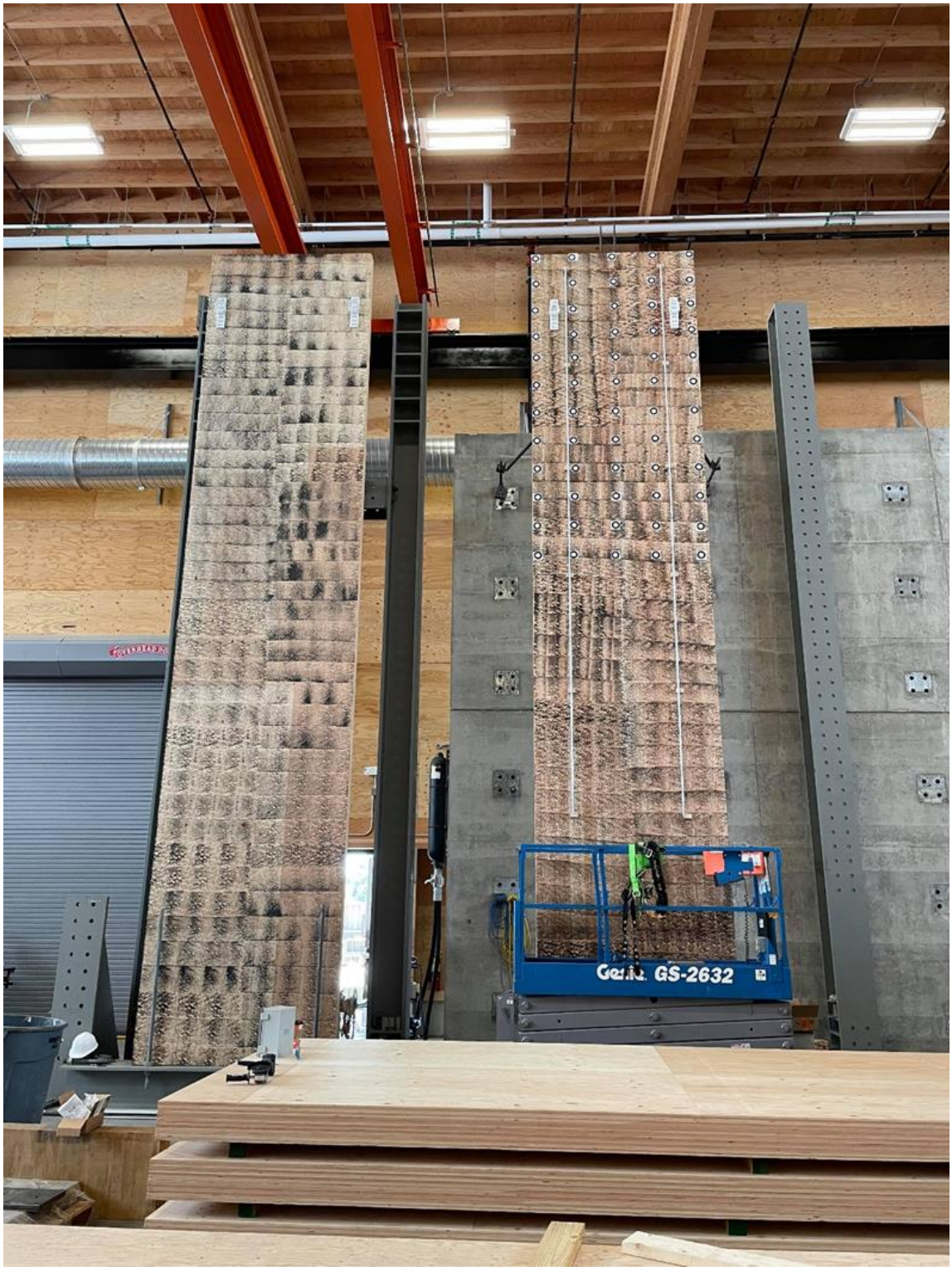

Figure 4.9. Erected MPP (left) and CLT (right) walls during instrumentation of rods, LVDTs, and targets

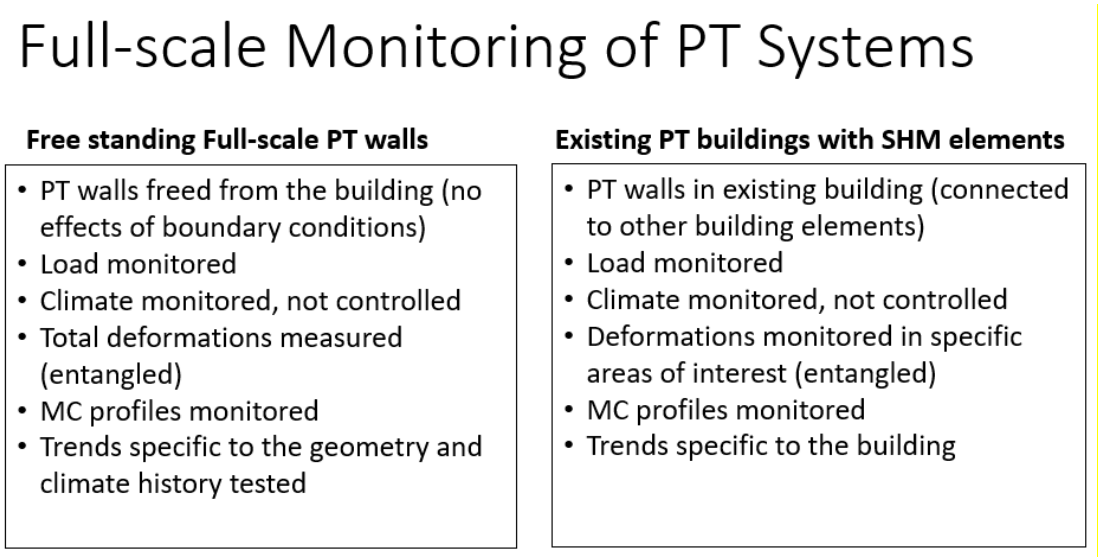

Figure 4.10. Full-scale monitoring of post-tensioned systems occurs as free-standing walls and the post-tensioned walls in an existing building

4.4.1 Full-scale Cross-laminated Timber Wall Design

The 5-ply CLT wall is 8.5 m tall and 1.8 m wide with a thickness of 0.174 m (28 ft x 6 ft x 6.8 in) (Figure 4.11). It contains two hollow chases down the length of the wall to provide space for the internal unbonded steel rods. The wall sits on a (72 in x 14 in x 1.75 in) steel plate with 29 mm (1.125 inch) openings, welded (3/8” E70 edge welded) to a beam (MCx40) to act as the foundation. The beam includes six stiffener plates welded to the web of the beam to prevent deflections. The beam contains two openings that line up with the steel plate openings and CLT chases, so the rods are secured (Figure 4.12).

Each 25.4 mm (1 in) diameter internal rod includes two coupler nuts that serve to connect three 3 m (10 ft) long rods to span the entire height of the panel while still allowing excess rod to protrude out the top of the panel for tensioning.

4.4.2 Full-scale Mass Plywood Panel Wall Design

The 6-inch MPP wall is 8.5 m tall and 1.8 m wide with a thickness of 0.152 m (28 ft x 6 ft x 6 in). This system has two external threaded steel rods, with a 25.4 mm (1 in) diameter along the middle of the wall and secured into a beam connected to a strong

floor. The rods for MPP are external due to manufacturing limitations with an inability to create internal hollow chases in a time-efficient process. The steel beam base contains two openings that align with the openings in the top steel plate, so the rods are secured (Figure 4.13 and Figure 4.14). The wall is connected to an H-frame, instead of the strong wall, so lab space can be used for other tests. It is connected by four rods that allow for vertical wall movement.

Each 25.4 mm (1 in) diameter internal rod includes two coupler nuts that serve to connect three 3 m (10 ft) long rods to span the entire height of the panel while still allowing excess rod to protrude out the top of the panel for tensioning.

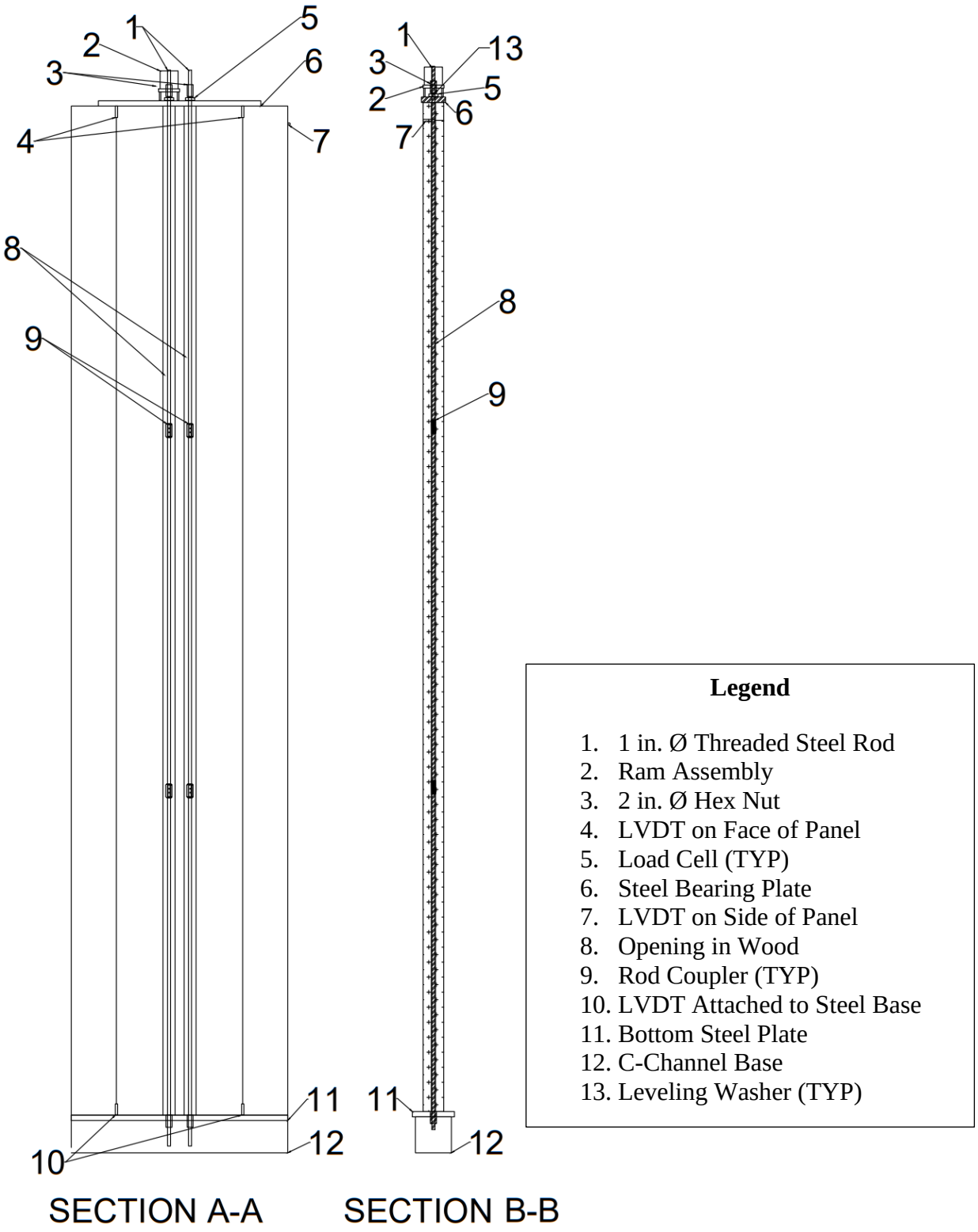

Figure 4.11. Drawings of the full-scale CLT wall with elevation and section views (credit: E. Baas)

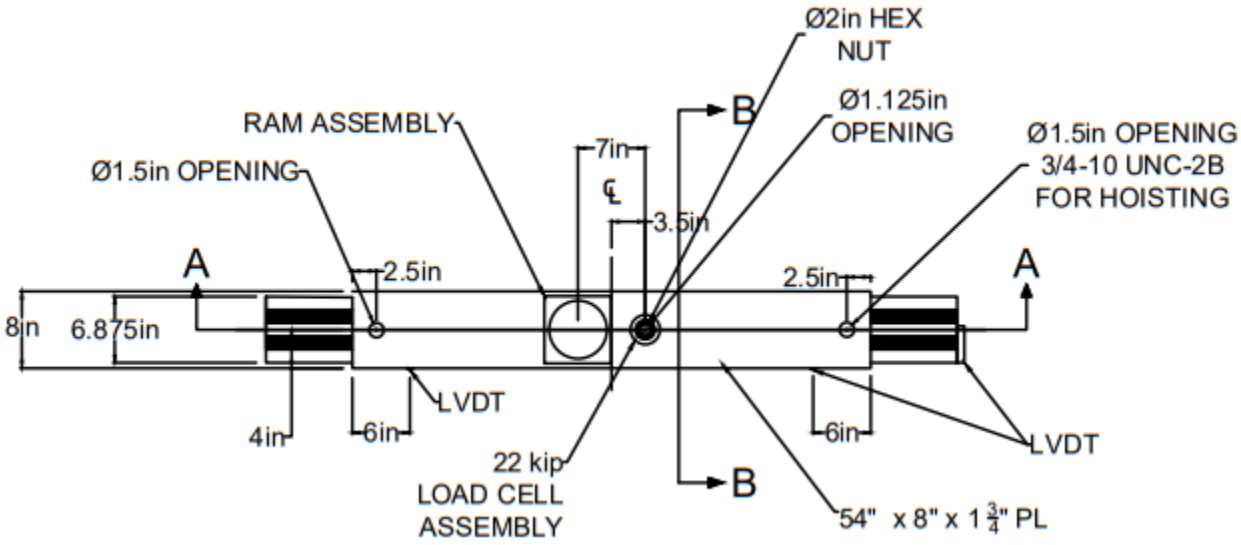

Figure 4.12. Plan view of CLT wall (credit: E. Baas)

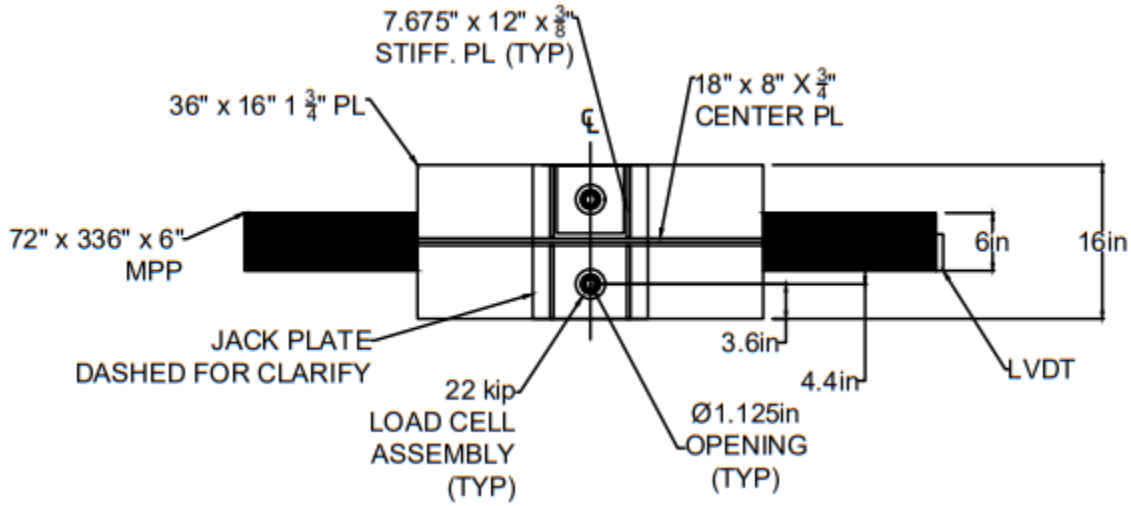

Figure 4.13. Plan view of MPP wall (credit: E. Baas)

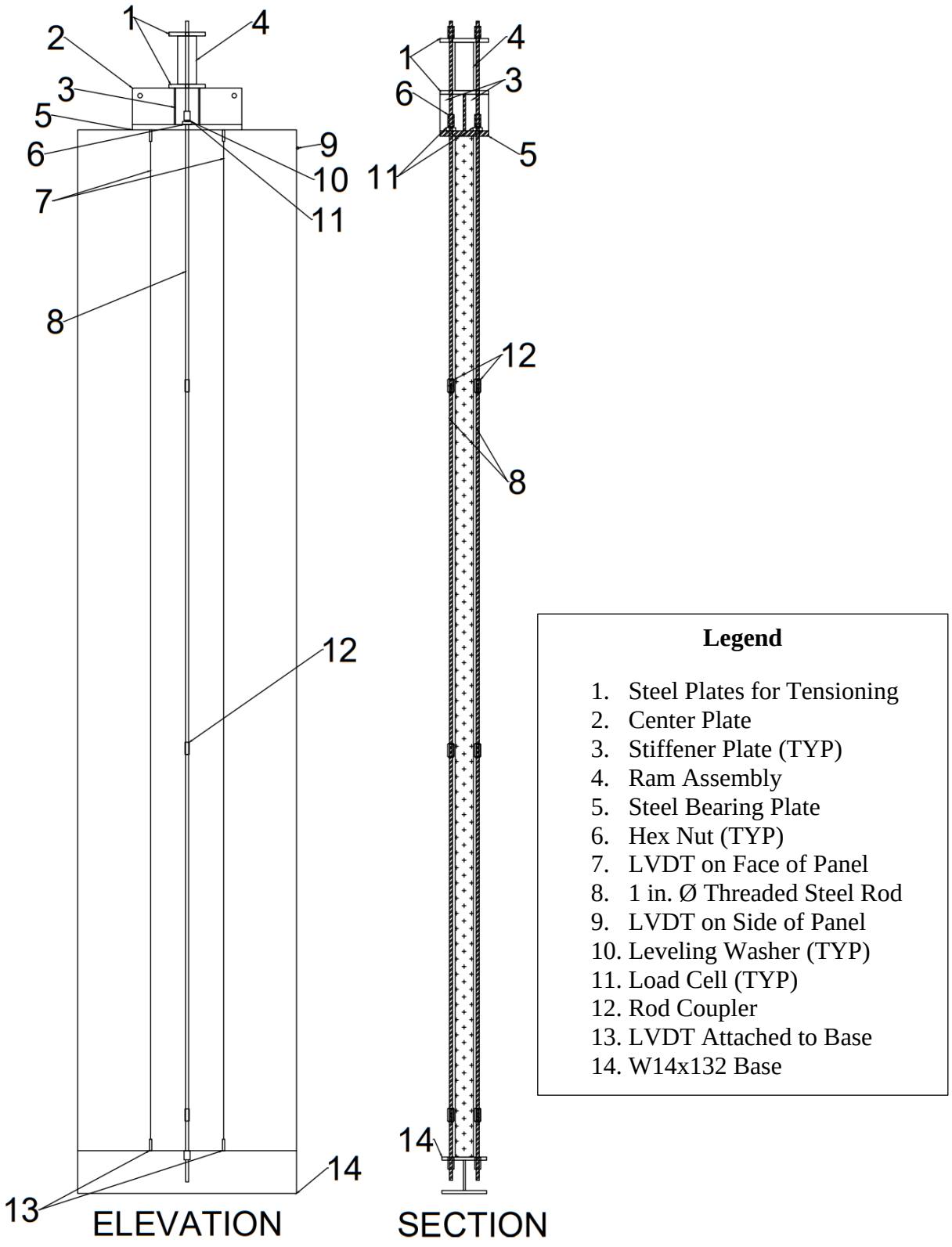

Figure 4.14. Drawings of the full-scale MPP wall with elevation and section views (credit: E. Baas)

The measurements of the full-scale PT walls provide strain, PT load, and environmental data for PT CLT and MPP walls for 52 weeks. Additionally, the panel dimensions are expected to fluctuate as they try to reach an EMC. The data collected from these walls are useful for refining a future material model that includes the entangled effects of PT loss and creep.

4.5 Conclusions

Two test scales have been proposed to analyze entangled effects affecting the long-term performance of post-tensioned CLT and MPP shear walls. The small-scale creep tests are designed to measure the creep of CLT and MPP under constant loads, therefore, separating the effects of tension losses. For this purpose, the spring base is designed to mitigate PT loss and keep the compressive load on the timber panels constant. The varying environment creep test is designed to trigger the mechano-sorptive effect, resulting in a superimposition of mechano-sorptive creep, viscoelastic creep, and shrinkage and swelling due to changes in moisture content. The deformations of unloaded specimens in the varying environment are recorded so that shrinkage and swelling data can be subtracted from the overall strain from loaded specimens to reveal creep data. The data collected from the constant environment test do not include the mechano-sorptive effect, so this data can be subtracted from the varying environment creep test to reveal mechano-sorptive creep data. In the end, viscoelastic creep, mechano-sorptive creep, and shrinkage and swelling of CLT and MPP panels will be identified and used to refine the material model.

The monitored full-scale post-tensioned timber walls record the total deformations, without separating creep, tension loss and environmental effects. In fact, the CLT and MPP walls do not contain a spring base, allowing for PT loss in response to creep. The role of creep resulting in PT loss is examined, providing long-term data of the intertwined variables.

Together, the small-scale tests provide the material data needed to refine a creep model. Then, the model can be updated to include a varying load and changing creep rate based on the data collected from the monitored full-scale walls.

5 TOWARDS A DIGITAL TWIN FOR MONITORING IN-SERVICE PERFORMANCE OF POST-TENSIONED SELF-CENTERING CROSS-LAMINATED TIMBER SHEAR WALLS

Overview

This chapter explains the need for building information models (BIM) of mass timber post-tensioned shear walls that can incorporate long-term data to predict creep and tension loss to support structural health monitoring (SHM) and long-term management of PT mass timber walls. This research includes a methodology for creating a BIM to assist with monitoring the long-term performance of post-tensioned mass timber shear walls. A case study is presented to assess the applicability of the proposed methodology for creating a digital shadow. This research works towards creating a digital twin, but it is more accurately described as a "digital shadow" because the digital model can be statically updated with long-term data and does not contain dynamic data integration and autonomous features such as alerting building managers when a high wood moisture content is recorded (Sepasgozar 2021).

5.1 Introduction

5.1.1 Structural Health Monitoring

Structural health monitoring (SHM) is generally defined as a damage detection strategy consisting of a network of sensors, a data acquisition system, and algorithms for data analysis (Li 2016). Structural health monitoring programs are being implemented into mass timber buildings as they gain popularity to document the performance of relatively new engineered wood products (EWPs). Examples of monitored mass timber buildings in North America include Brock Commons in Vancouver, BC, Canada (Mustapha 2017), and the Wood Innovation and Design Centre in Prince George, BC, Canada (Hu 2015). Monitored buildings featuring post-tensioned mass timber shear walls, include Peavy Hall in Corvallis, Oregon, USA (Baas et al. 2021a), Trimble New Zealand Office in Christchurch, NZ (Granello 2020), and the Nelson Marlborough Institute of Technology in Nelson, NZ (Morris 2011). In addition to common dynamic and quasi-static measurands in steel and concrete buildings (e.g., acceleration, strains, displacements), wood buildings require

particular attention to environmental parameters as well. Wood is a hygroscopic material that reacts to changes in humidity and temperature (Skarr 1983). The service life of timber systems can be negatively impacted by an increase in wood moisture content due to the climate or exposure to water. An increase in wood moisture content results in swelling, strength reduction, increased creep, and increased likelihood of decay fungi and pests (Skarr 1988, Glass 2010).

Monitoring post-tensioned timber buildings supports the ease and speed of corrective and preventative maintenance of the structural system. However, many important measurands such as wood moisture content and tension loss are difficult to quantify without sensors. Sensor outputs may not provide intuitive information to an untrained building manager, since making sense of data is facilitated when data are analyzed in a context (e.g., Napolitano 2018). Additionally, identifying the location of each sensor can prove to be a difficult task, especially when sensors are in inaccessible areas. The serviceability of timber structures can be improved through SHM practices paired with a visualization tool, such as a digital model.

5.1.2 Building Information Modeling

Despite widespread use of BIM during design and construction, they are not always used to their full capabilities upon the completion of a construction project. Full benefits of BIMs can be realized throughout the lifecycle of facilities as they can be used for SHM, maintenance, storage for cultural and historical documentation, and deconstruction. For these scopes, BIMs can be used to incorporate service life data, such as continuous data from sensors or a routine inspection of built facilities (Boje 2020).

Recently BIM has been proposed as a tool to document heritage sites in a digital format and assist with maintenance and retrofitting (Godinho et al. 2020). In fact, there is an opportunity for cultural heritage buildings to benefit from BIM by modeling and documenting architectural elements, as well as maintenance operations, information from periodic inspections, and data from instrumental tests (Pocobelli 2018). In general, this requires static integration of data into BIM over different time periods. In addition, many heritage sites have complex and unusual geometry that is

not represented in parametric geometries included in object libraries in BIM software (Godinho et al. 2020). In addition, graphic documentation of many historical buildings can be scarce or completely missing. Scan-to-BIM approaches have been proposed in these cases to capture the architecture and design in an effort to preserve historical buildings (Yan et al. 2015).

Scan-to-BIM is one of the methods used when there is a need of accurate spatial data describing the as-built state, rather than the design model. This is the case when BIMs are used for managing facilities. Alternative methods of gathering spatial data exist and method selection may depend on the specific project accounting for instrument availability, cost, and other factors. For example, Lu et al. (2020) developed a geometric model based on images and CAD drawings. A scan-to-BIM approach is a possible technique for creating a BIM of an existing building through LiDAR scanning. LiDAR is a remote sensing method that uses light to measure distances and collect 3D data in the form of a point cloud (NOAA 2021). The scan-to-BIM approach is useful for obtaining accurate models of existing structures that do not have a BIM or have changed since the BIM was created. Reasons for a BIM not accurately reflecting the built environment could be due to change orders during construction, or the addition of appliances and furniture, renovations, or even the addition of sensors.

Inadequate interoperability and incompatibility between design, engineering, facilities management, and business processes software systems resulted in a $15.8 billion total added cost in the construction industry, according to a study conducted by the National Institute of Standards and Technology (NIST) (Gallaher et al. 2004). The Industry Foundation Classes (IFC), an International Organization for Standardization (ISO) standard designed to deal with the industry's interoperability problem, allows information to be transferred from one tool to the next. However, IFC does not work seamlessly across all application domains (ISO 2018). Semantic information, such as parameters measured from sensors, may become lost when IFC files are transferred to other applications.

Current facility management information systems are complex and provide high-quality data important for maintenance. However, these systems lack

interoperability and visualization capabilities. Shalabi and Turkan (2017) presented an automated process that responds to alarms from facility management systems such as building energy management systems (BEMS) or building automation systems (BAS). It works by collecting detected alarms from facility management systems and retrieves the maintenance information to support corrective maintenance actions. While this work is beneficial for improving the operation and management of built facilities, the concept can be improved through intuitive visuals (Shalabi and Turkan 2017).

5.1.3 Digital Twins

Grieves (2014) gives a holistic view of the complex system representing a DT and lists the main components as:

1) the physical object,
2) the digital model, and
3) data that connects them.

The physical object, such as a building, is instrumented such that sensors collect data that is used to inform digital models. Engineering or physical models embedded into the digital model can be paired with artificial intelligence (AI), or other probabilistic simulations, to discover information needed to manage data from the physical world or represent how a structure may respond to various loading and environmental conditions (Grieves 2014). For example, a physical model linking environmental or moisture data to wood decay models could provide semantic information such as labeling a moisture content as “high”, given the environmental conditions. Or a model could provide a prediction of PT loss over time, given parameters regarding creep rate, compressive load on timber, and timber moisture content fluctuations.

Data integration between the physical and digital model is identified as one of the greatest challenges when creating a DT and can arise from the lack of data interoperability among domains as well as varieties of data and sensors, including type, nomenclature, and format (Lamb 2019).

Several studies investigated integrating sensor data with a BIM for a variety of purposes. For example, Attar et al. (2010) created a real-time building performance

visualization using wireless sensor networks. Sensor outputs provided visualization through shaded and highlighted objects within a software developed by Autodesk. No structural information or sensor specifications were added to the model.

Theiler and Smarsly (2018) extended the IFC schema to describe monitoring-related information so that all information needed for SHM are contained in an IFC-based BIM. This study focused on allowing SHM information to be accurately transferred across multiple platforms but was not implemented in a real SHM project. In several proposed frameworks, applications were developed, or existing software was paired with the geometric information obtained from a BIM (Suprabhas 2017).

Despite a vast array of useful data to document mass timber building performance, extensive efforts are required to process and visualize data in one platform (Baas et al. 2021b). Managing recording devices, matching sensor output to a specific location, and processing sensor readings into useful data is a time-consuming necessary task. However, an opportunity to improve upon data management, visualization, and use through a digital model that can automatically notify building management of maintenance concerns, still exists (Baas et al. 2021b).

Therefore, the goal of this study is to work towards creating a BIM that accurately represents the as-built spatial information of a building that is enriched with sensory data to improve the visualization of SHM practices to assist with maintenance decisions.

5.2 Methodology for Creating a Building Information Model for Structural Health Monitoring

The general methodology for creating a building information model to assist with structural health monitoring is outlined below:

5.2.1. Obtain geometric information expressed as a BIM

Building Information Models may be obtained from the architect, owner, or general contractor of a building. Numerous measurements could provide enough information to create a BIM through Revit or SketchUp. Architectural drawings may contain enough detailed information to create a BIM but might not reflect any changes to the

building that occurred after the drawings. A scan-to-BIM approach provides very accurate measurements of existing buildings but is an expensive and technical approach.

5.2.2. Attribute the Model with Structural Information

Structural information such as wood and steel grades can be included for each building element under the *Properties* tab in Revit. The manufacturer's website, data sheets, and construction manuals are useful for gathering information regarding the grade, design parameters, and strength of materials. Additionally, the wall material properties can be modified to match the appearance of the physical elements.

5.2.3. Add Virtual Sensors in IFC-BIM

Virtual sensors should be modeled based on their location in the physical building. Each sensor type is defined as a subcategory of the Specialty Equipment category within Revit. In Revit import IFC options, *IfcSensor* and *IfcSensorType* are within the Specialty Equipment category (Valinejadshoubi 2017). Each sensor type should be modeled as a separate family component and added as a subcategory within the *Object Styles* window of Revit. This allows the sensors to be identified within the IFC file for future applications. Under the *Properties* tab, the manufacturer, model information, and location of each sensor can be specified. Additional information regarding the sensors can be stored online and linked to the model. It is beneficial to include a webpage link that can provide sensor specifications such as measuring range, tolerance, location, and installation date.

5.2.4. Link Virtual Sensors to Real Sensor Data

The IFC schema lacks modeling capabilities that would be useful for displaying monitoring-related information (Rio 2012). Other software or Revit add-ons exist to assist with displaying data, but can be expensive, may require programming, or risk interoperability issues. However, Revit 2020 includes Dynamo, a visual programming platform that can be paired with a specific Application Programming Interface (API) that allows sensory data to be accessed and displayed through Revit (Desogus 2021).

A Specialty Equipment Schedule provides a list of the sensors so their specifications, locations, and historical monitoring data can easily be accessed if monitoring data is displayed on the internet.

5.3 Case Study: The George W. Peavy Forest Science Center

The George W. Peavy Forest Science Center, or "Peavy Hall", is a mass timber building at Oregon State University (OSU) that was used as a case study for this project. The building contains cross-laminated timber (CLT)-concrete composite floors, glulam beams and columns, a mass plywood panel (MPP) roof system, and CLT post-tensioned (PT) self-centering shear walls. Peavy Hall is the world's first application of cross-laminated timber post-tensioned self-centering shear walls, also known as "rocking" walls. There are 41 self-centering shear walls with unbonded steel rods secured in the foundation. Each wall contains four internal rods located in four hollow chases down the length of the panel. During construction, the top of the rods was tensioned using a hydraulic jack and hex nuts to transfer a compressive force along the steel bearing plate so the center of the wall is compressed. U-shaped flexural plates (UFPs) between the walls were designed to bend and yield during an earthquake as they help dissipate the seismic energy (Kelly et al. 1974).

The building is equipped with over 350 sensors, which include load cells, string potentiometers, resistance-type moisture meters, relative humidity sensors, and thermistors. These sensors monitor tension losses in PT steel displacements and deformations of PT shear walls, wood moisture content, and microclimate in the monitored areas (Figure 5.1) (Baas et al. 2021a). These parameters are all important to monitor creep and PT loss in the shear walls.

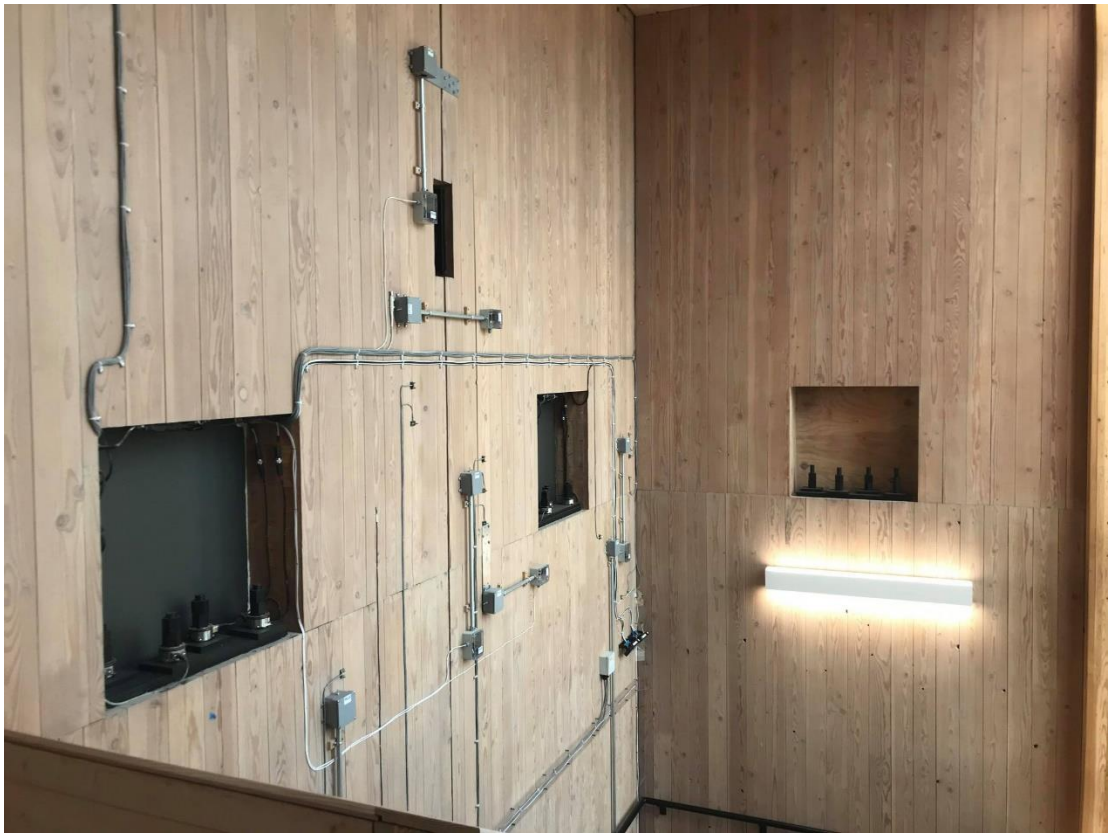

Figure 5.1. Sensors placed on PT CLT walls in Peavy Hall, Oregon, USA.

In this study, the east stairwell of Peavy Hall was chosen to implement a digital shadow because this location includes an extensively monitored pair of post-tensioned CLT self-centering shear walls. Sensors in these walls monitor tension loss of all four steel PT rods in each of the shear walls, wood moisture content at varying depths and locations, and whole wall deformations resulting from superimposition of creep and moisture movement as well as indoor environmental conditions. Additional string potentiometers are used to evaluate residual displacements in the walls after an earthquake (Baas et al. 2021a).

Although an existing BIM existed for Peavy Hall, it was outdated due to changes during construction and the addition of sensors. An accurate geometric model of the east stairwell of Peavy Hall was generated through a scan-to-BIM approach. LiDAR was used due to instrument availability as well as the need for a more precise model. The Leica ScanStation P40 LiDAR system scanned the east stairwell of Peavy Hall to create a point cloud that includes three CLT post-tensioned

walls instrumented with load cells, string potentiometers, and moisture meters (Leica Geosystems 2021). Point clouds from ten locations within the east stairwell of Peavy Hall were collected. Twenty-five targets were used to register the point clouds to develop a cohesive and precise model that included the sensors installed in the shear walls for SHM purposes (Figure 5.2). Erroneous and unwanted data points caused by light reflection from windows and data points beyond the east stairwell were removed within the Cyclone software (Leica Geosystems 2021).

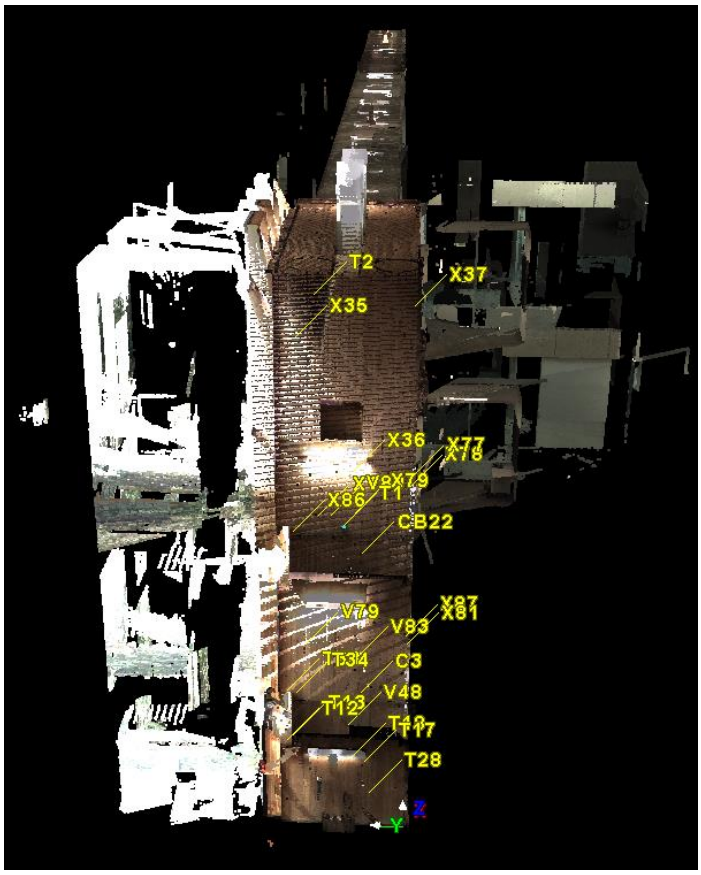

Figure 5.2. Target locations used to register the point clouds to become a cohesive model

The point cloud of the east stairwell of Peavy Hall was processed using Cloudworx, a Revit add-on (Figure 5.3) (Leica Geosystems 2021). Cloudworx runs Cyclone in the background which allows users to import point clouds into the Autodesk Revit environment. Levels were created by manually selecting points at each floor in the point cloud (Figure 5.4). In areas where the points appeared sparse, the view range was adjusted to capture the view of additional points so the walls

could be placed accurately. The levels were viewed simultaneously to ensure the modeled stairs aligned with adjacent levels as a validation check (Figure 5.5). Wood and steel grades were included for each building element under the *Properties* tab in Revit (Figure 5.6).

Figure 5.3. Building Information Model (left) and point cloud model (right)

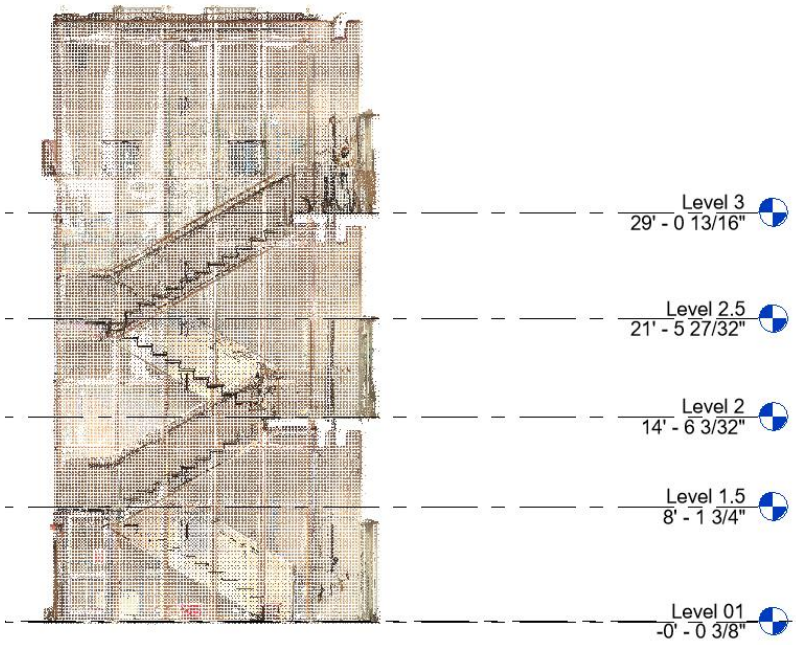

Figure 5.4. Levels created by picking points within the virtual model

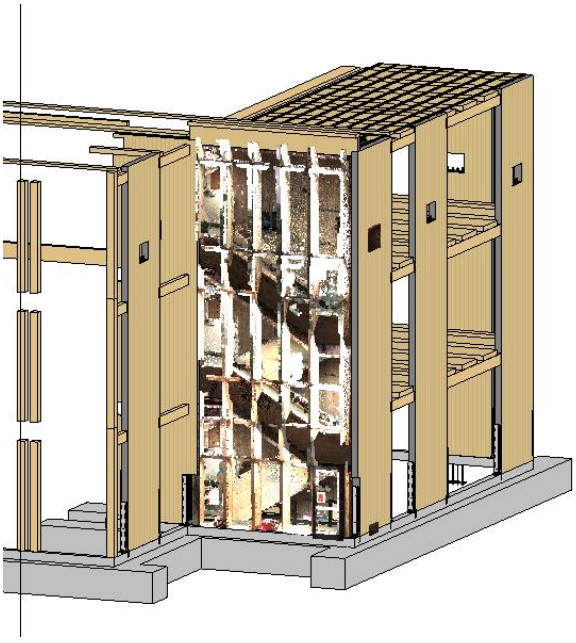

Figure 5.5. Point cloud fits within existing BIM for comparison and verification of correct units

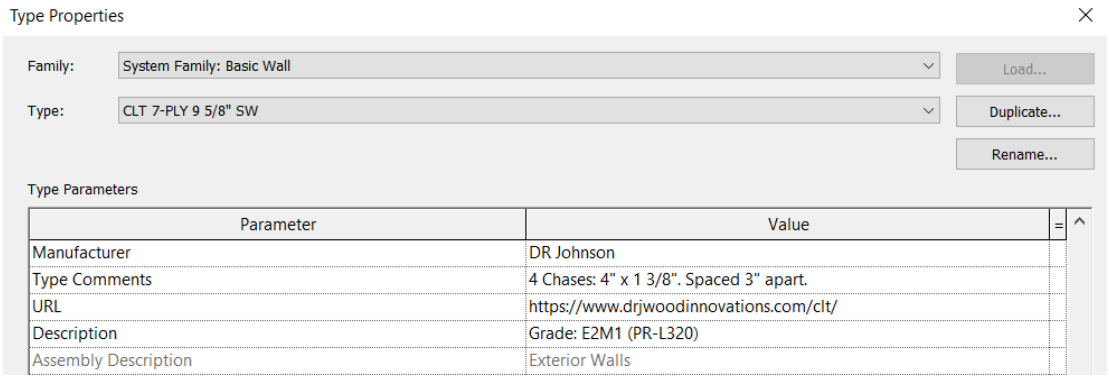

Figure 5.6. Materials contain additional information under the Properties tab regarding the grade, dimensions, and comments

Virtual sensors were modeled based on their location in the point cloud (Figure 5.7). Each sensor type was defined as a subcategory of the specialty equipment category within Revit. In Revit import IFC options, *IfcSensor* and *IfcSensorType* were within the specialty equipment category (Figure 5.8) (Valinejadshoubi 2017). Each sensor type was modeled as a separate family component and added as a subcategory within the *Object Styles* window of Revit. This allows the sensors to be identified within the IFC file for future applications. The virtual sensors were modeled as an enlarged version of the physical sensors to increase visibility. Under the *Properties* tab, the manufacturer, model information, and location of each sensor were specified. The model information includes a webpage link that provides sensor specifications such as measuring range, tolerance, location, and installation date (Figure 5.9).

Figure 5.7. Point cloud view shows sensors in east stairwell

*exportlayers-ifc-IAI.txt - Notepad

File Edit Format View Help

```
Site    Property Lines  IfcSite
Site    Survey Point    IfcSite
Site Tags               Not Exported
Spaces          IfcSpace
Spaces  Color Fill      IfcSpace
Spaces  Interior        IfcSpace
Spaces  Reference       IfcSpace
Specialty Equipment     String Pot      IfcSensorType
Specialty Equipment     Load Cell       IfcSensorType
Specialty Equipment     MC Sensor       IfcSensorType
Specialty Equipment     Hidden Lines    IfcBuildingElementProxy
Specialty Equipment Tags                Not Exported
Spot Coordinates                Not Exported
Spot Elevations         Not Exported
Spot Slopes             Not Exported
Sprinklers              IfcFireSuppressionTerminalType
Stair Landing Tags              Not Exported
Stair Paths             Not Exported
Stair Paths     <Above> Up Arrows
Stair Paths     Down Arrows
```

Ln 334, Col 44 | 100% | Windows (CRLF) | UTF-16 LE

Figure 5.8. Sensor names are specified under the Specialty Equipment category

Sensor_Specifications | Sensor_Information

Show rows with cells including:

Sensor Type	Quantity	Measuring Range	Tolerance
Resistance-Type Moisture Meter with Insulated Electrode Pins	111	9% to 30%	±1%
String Potentiometer	10	±50mm	0.1mm
MF52 Thermistor	7	-55°C to 125°C	±1%
HTM2500 Relative Humidity Gauge	3	1% to 99%	±3 to 5%
Load Cell	28	Unknown	Unknown
Davis Vantage Pro2 Weather Station	1	Dependent on measurand, see data platform files	
Data Acquisition Unit	16	TMP: 0°C to 40°C	TMP: ±1 °C
		RH: 5% to 100%	RH: ±5%

Figure 5.9. Sensor specifications provided by a link to the table that displays the measuring range and tolerance for all the sensors in the building (OSF 2021)

The monitoring data acquired from Peavy Hall is displayed on the internet through Open Science Framework (OSF 2021). Although real-time sensor data is not accessible from the open-access OSF platform, historical sensor data collected during construction from May 8th, 2019 to March 10th, 2020, when all the walls in the building were post-tensioned, is stored and displayed graphically. Each virtual sensor within the BIM was linked to its corresponding data on OSF to improve data management and visualization. Clicking on an individual sensor within the BIM reveals the *Properties* window that includes the webpage link to visualize its data, the manufacturer's website, model information, and a description of the location of the sensor. The Specialty Equipment Schedule is a table that lists all sensors along with their *URL*, *Manufacturer*, *Model*, and *Comments* fields (Figure 5.10). If a row is selected, that sensor is highlighted within the BIM. This solution allows descriptive sensors to be visualized and contain a URL that displays the data collected by that sensor (Figure 5.11).

{3D} Specialty Equipment Schedule

<Specialty Equipment Schedule>

A	B	C	D	E
Family	URL	Manufacturer	Model	Comments
Load Cell	https://osf.io/ehm	http://www.vishaypg	https://osf.io/j4rzd/	Mulit-axial strain guage
Load Cell	https://osf.io/ehm	http://www.vishaypg	https://osf.io/j4rzd/	Mulit-axial strain guage
Load Cell	https://osf.io/ehm	http://www.vishaypg	https://osf.io/j4rzd/	Mulit-axial strain guage
Load Cell	https://osf.io/ehm	http://www.vishaypg	https://osf.io/j4rzd/	Mulit-axial strain guage
Load Cell	https://osf.io/r5d	http://www.vishaypg	https://osf.io/j4rzd/	Mulit-axial strain guage
Load Cell	https://osf.io/r5d	http://www.vishaypg	https://osf.io/j4rzd/	Mulit-axial strain guage
Load Cell	https://osf.io/r5d	http://www.vishaypg	https://osf.io/j4rzd/	Mulit-axial strain guage
Load Cell	https://osf.io/r5d	http://www.vishaypg	https://osf.io/j4rzd/	Mulit-axial strain guage
MC sensor	https://osf.io/9sw	https://www.smtres	https://osf.io/j4rzd/	PLY 1
MC sensor	https://osf.io/9sw	https://www.smtres	https://osf.io/j4rzd/	PLY 1
MC sensor	https://osf.io/9sw	https://www.smtres	https://osf.io/j4rzd/	PLY 1
MC sensor	https://osf.io/9sw	https://www.smtres	https://osf.io/j4rzd/	PLY 1
MC sensor	https://osf.io/9sw	https://www.smtres	https://osf.io/j4rzd/	PLY 1
MC sensor	https://osf.io/9sw	https://www.smtres	https://osf.io/j4rzd/	PLY 2
MC sensor	https://osf.io/9sw	https://www.smtres	https://osf.io/j4rzd/	PLY 2
MC sensor	https://osf.io/9sw	https://www.smtres	https://osf.io/j4rzd/	PLY 2
MC sensor	https://osf.io/9sw	https://www.smtres	https://osf.io/j4rzd/	PLY 3
MC sensor	https://osf.io/9sw	https://www.smtres	https://osf.io/j4rzd/	PLY 4
MC sensor	https://osf.io/9sw	https://www.smtres	https://osf.io/j4rzd/	PLY 4
MC sensor	https://osf.io/9sw	https://www.smtres	https://osf.io/j4rzd/	PLY 4
MC sensor	https://osf.io/9sw	https://www.smtres	https://osf.io/j4rzd/	PLY 4
MC sensor	https://osf.io/9sw	https://www.smtres	https://osf.io/j4rzd/	PLY 4
MC sensor	https://osf.io/9sw	https://www.smtres	https://osf.io/j4rzd/	PLY 4
MC sensor	https://osf.io/9sw	https://www.smtres	https://osf.io/j4rzd/	PLY 4
MC sensor	https://osf.io/9sw	https://www.smtres	https://osf.io/j4rzd/	PLY 4
MC sensor	https://osf.io/9sw	https://www.smtres	https://osf.io/j4rzd/	PLY 6
MC sensor	https://osf.io/9sw	https://www.smtres	https://osf.io/j4rzd/	PLY 6
MC sensor	https://osf.io/9sw	https://www.smtres	https://osf.io/j4rzd/	PLY 6
MC sensor	https://osf.io/9sw	https://www.smtres	https://osf.io/j4rzd/	PLY 6
MC sensor	https://osf.io/9sw	https://www.smtres	https://osf.io/j4rzd/	PLY 6
MC sensor	https://osf.io/9sw	https://www.smtres	https://osf.io/j4rzd/	PLY 7
MC sensor	https://osf.io/9sw	https://www.smtres	https://osf.io/j4rzd/	PLY 7
MC sensor	https://osf.io/9sw	https://www.smtres	https://osf.io/j4rzd/	PLY 7
MC sensor	https://osf.io/9sw	https://www.smtres	https://osf.io/j4rzd/	PLY 7
MC sensor	https://osf.io/9sw	https://www.smtres	https://osf.io/j4rzd/	PLY 7
SP-1	link data	https://www.smtres	https://osf.io/j4rzd/	Top vertical
SP-2	link data	https://www.smtres	https://osf.io/j4rzd/	Top horizontal
SP-3	link data	https://www.smtres	https://osf.io/j4rzd/	Middle
SP-4	link data	https://www.smtres	https://osf.io/j4rzd/	Middle horizontal
SP-5	link data	https://www.smtres	https://osf.io/j4rzd/	East Wall
SP-6	link data	https://www.smtres	https://osf.io/j4rzd/	Long East
SP-7	link data	https://www.smtres	https://osf.io/j4rzd/	Long West
SP-8	link data	https://www.smtres	https://osf.io/j4rzd/	Long West
SP-9	link data	https://www.smtres	https://osf.io/j4rzd/	Bottom middle
SP-10	link data	https://www.smtres	https://osf.io/j4rzd/	Bottom East

Figure 5.10. The Specialty Equipment Schedule in Revit lists all modeled sensors, the URL to see their data, a link to a table that provides sensor model specifications, and comments

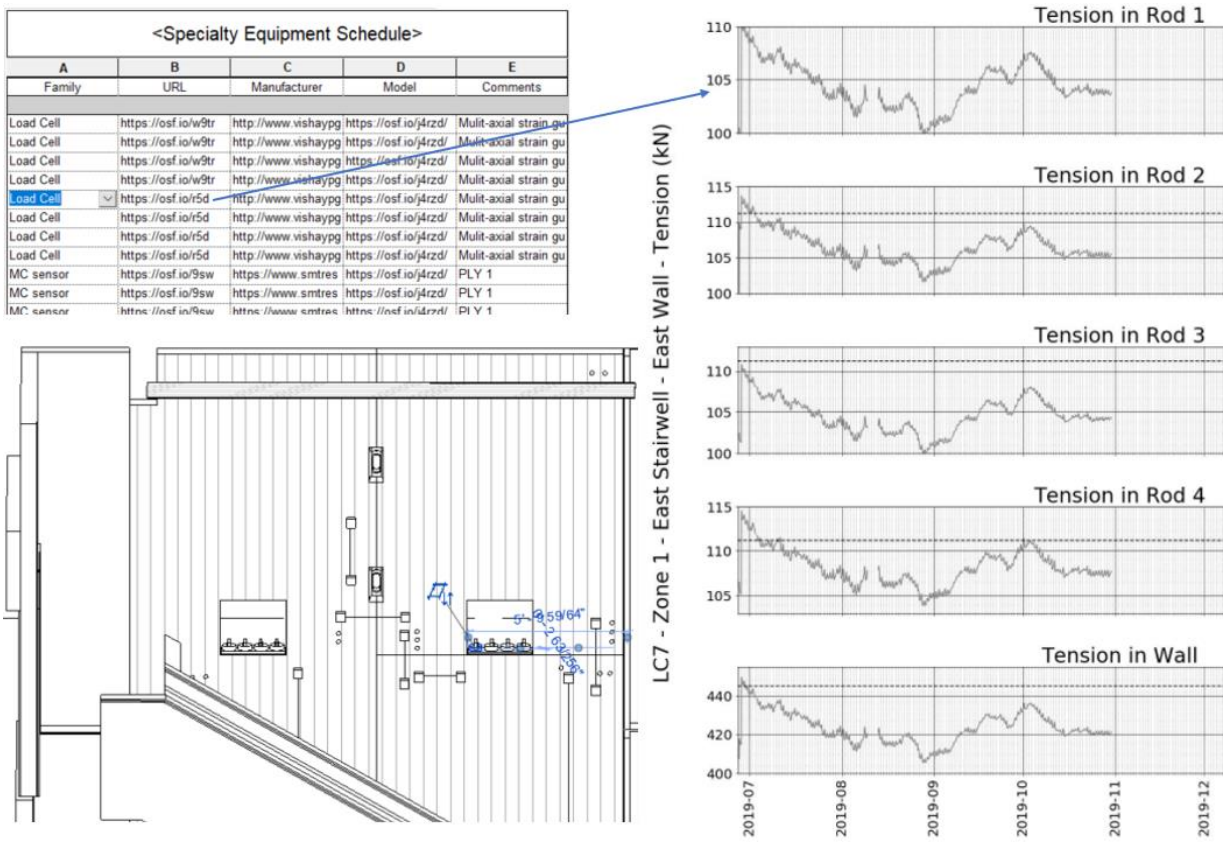

Figure 5.11. The selected load cell in the Specialty Equipment Schedule becomes highlighted in the model (bottom left). Clicking on the URL within the schedule displays the sensor data in a new window (right).

5.4 Conclusions, Limitations, and Future Work

The as-built BIM of the east stairwell of Peavy Hall was developed using Revit software and the Cloudworx plugin and enhanced with structural information and sensor specifications. A Specialty Equipment Schedule provided a list of the sensors so their specifications, locations, and historical monitoring data could easily be accessed. This work is not a dynamic digital model because live data from Peavy Hall is not sent to the digital model to assist with real-time control tasks, such as automatically alerting building managers when a sensor records a high moisture content or a large drop in rod tensile force. Instead, the static digital model can be

updated periodically as long-term data about a physical asset is added. This work towards a digital twin, is sometimes referred to as a “digital shadow” to differentiate it from a dynamic digital model (Kritzinger et al. 2018). The precise placement of these sensors and the possibility to associate the measured parameters of these entities within a BIM is hypothesized to assist with data management by adding a spatial element to data and analysis results, which could lead to the prolonged service life of a building. Future work can focus on linking the BIM to live sensor data to create a dynamic model capable of alerting building stakeholders about maintenance concerns. In addition, the integration of viscoelastic and mechano-sorptive models, as well as of tension loss models into BIM can assist in the future with the design, construction, and maintenance of mass timber post-tensioned shear walls.

6 OVERALL CONCLUSIONS, LIMITATIONS, AND FUTURE WORK

6.1 Conclusions

A literature review regarding the creep of cross-laminated timber and mass plywood panels axially loaded in compression revealed the lack of published studies and understanding of the creep characteristics of these engineered wood products that lead to tension loss when designed as a post-tensioned timber rocking shear wall.

The primary objectives of this research were accomplished by a preliminary material model for the creep of wood, methodologies to measure the in-plane creep of cross-laminated timber and mass plywood panel and monitor the creep and PT loss of full-scale timber walls, and a methodology for creating a building information model to assist with visualizing the performance of post-tensioned mass timber shear walls.

The material point method (MPM) was used to model the creep deformation of wood as a transversely isotropic material. The model was fitted with data from a previous experimental study (Hu and Guan 2018). The longitudinal and transverse directions fit well, but many more viscoelasticity experiments are needed to refine all the possible time-dependent parameters. A new approach to modeling mechano-sorptive creep was proposed. The shift-factor method reimagines mechano-sorption as part of a material's viscoelastic relaxations rather than a separate mechanical mechanism seen only in wood. This creep model is only a preliminary step if the end goal is a model that predicts the PT loss of post-tensioned timber shear walls. This model can be improved by the results from the creep and full-scale PT tests.

A separate methodology for a constant environment creep test and varying environment creep test were included so that the mechano-sorptive effect due to changes in wood moisture content can be identified. The small-scale creep tests were designed to capture important creep behavior on the material scale. These creep tests provide material data, such as tensions force of the rods, deformation of the panels, and wood moisture content profiles, important for understanding the viscoelastic and mechano-sorptive creep characteristics of EWPs subjected to in-plane axial loads.

Long-term, full-scale post-tensioned CLT and MPP walls were designed to analyze the entangled effects of creep and tension loss in an uncontrolled and realistic environment. Digital Image Correlation (DIC) was setup as a complementary non-

contact, full-field method to map the strain of the timber panels during tensioning, and throughout the duration of an entire year. These tests provide long-term monitoring data for CLT and MPP utilized as a structural system designed for seismic resiliency.

A methodology for creating a BIM to assist with visualizing data describing the long-term performance of post-tensioned mass timber shear walls was proposed. The approach was implemented to create a digital shadow of the east stairwell of Peavy Hall. A scan-to-BIM approach provided a very accurate digital model but registering the data and converting it into a BIM was very time consuming. The Revit add-on, Cloudworx, does not provide a sufficient, automated solution for converting points clouds into a BIM. Historic sensor data were available through a webpage URL specific to each sensor in the Revit model. The ease of correlating structural health monitoring data to a specific sensor can improve visualization for building management to assist with maintenance decisions. Additionally, if SHM data are intuitive and presented to the public, this allows occupants to be aware of upcoming maintenance activities, and allow them to make maintenance requests, improving the service life of the building.

Overall, the results of each objective provide the foundation for long-term tests, modeling, and monitoring of post-tensioned timber wall panels. Careful design of tests and data collection is imperative for obtaining useful data regarding creep, a relatively difficult to measure phenomenon. The tasks accomplished in this research provide a step towards increasing the fundamental understanding of viscoelastic creep, mechano-sorptive creep, and post-tension loss of mass timber walls and how the design of these systems can be improved and maintained for seismic resiliency.

6.2 Limitations

The methodologies were created based on the current knowledge of viscoelastic creep, mechano-sorptive creep, and PT structures. These methodologies cannot be validated yet but will be implemented in future studies. There are many mistakes or uncertainties that can occur during testing that could result in a failed experiment. Uncertainties in measurements are a threat to obtaining useful data. The accuracy of

sensors is very important for measuring extremely small deformations. LVDTs should have an adequate measuring range while the load cells should not be loaded above their capacity. The accuracy of sensors can be a limitation if noise provides larger readings than creep measurements. External sources may interrupt data such as vibrations or accidentally moving the specimens. These methodologies cover the design of specimens and experimental conditions, but actual oversight on collecting the data cannot be provided.

Limitations of this study include a lack of standard in-plane creep testing procedures for timber, and very few published studies measuring the creep of CLT, while none exist for MPP. A lack of published creep test data created a limitation on refining the creep model. The BIM was limited to displaying historical sensor data because the live readings are not available through the internet.

Many external limitations of this study were due to COVID-19. Laboratory shutdowns, reduced workforce, and supply chain issues greatly impacted the research schedule. Maintenance of the environmental chambers also affected the timeline for long-term tests.

6.3 Future Work

Future work involves implementing the methodology outlined for small-scale creep tests. Later, this data will be useful for refining the material properties for modeling the creep of engineered wood products using the MPM. The current model can only handle creep under a constant load and will have to be updated in numerous ways, such as accounting for changes in relative humidity, moisture content, and load, to become a model that can predict PT loss. Then the model can be validated against the data recorded from real SHM projects and updated for use as a predictive model Additionally, the digital shadow has potential to be converted into a digital twin if live sensory data is accessible through the internet. This would allow the BIM to become a dynamic model that can display live SHM data through a Revit add-on or another application. Lastly, embedding engineering models into a BIM to automatically alert building management of concerning sensory data is a topic of interest.

7 BIBLIOGRAPHY

American Wood Council (AWC). (2020). Tall Mass Timber. Accessed 12/21/2020 https://awc.org/tallmasstimber

ANSI/APA. (2019). PRG 320-2019: Standard for Performance Rated Cross-Laminated Timber. The Engineered Wood Association and Approved American National Standard.

APA (2021). Cross-Laminated Timber. Accessed August 20th, 2021. https://www.apawood.org/cross-laminated-timber

Armstrong, L.D. and R.S. Kingston. (1960). Effect of moisture changes on creep in wood. In: Nature, London, 185(4716), 862–3.

ASTM D4442-20, (2020). Standard Test Methods for Direct Moisture Content Measurement of Wood and Wood-Based Materials, ASTM International, West Conshohocken, PA, 2020, www.astm.org

Attar, R., E. Hailemariam, M. Glueck, A. Tessier, J. McCrae, A. Khan, (2010a), BIM-based Building Performance Monitoring, Proceedings of the SimAUD, Orlando, Florida, p.32.

Autengruber, M., Lukacevic, M., Gröstlinger, C., Eberhardsteiner, J., and Füssl, J. (2021). "Numerical Assessment of Wood Moisture Content-Based Assignments to Service Classes in EC 5 and a Prediction Concept for Moisture-Induced Stresses Solely Using Relative Humidity Data." *Engineering Structures* 245 (June): 112849. https://doi.org/10.1016/j.engstruct.2021.112849.

Baas, E.J., Granello, G., Barbosa, A.R., Riggio, M. (in press). Post-tensioned timber wall buildings: design & construction practice in New Zealand & United States. *WCTE*. 2021.

Baas, E.J., Riggio, M. and Barbosa, A.R., (2021a). Structural health monitoring data collected during construction of a mass timber building with a data platform for analysis. *Data in Brief*, *35*, p.106845

Baas, E. J., Riggio, M., & Barbosa, A.R. (2021b). A methodological approach for structural health monitoring of mass-timber buildings under construction. *Construction and Building Materials*, *268*, 121153.

Bardenhagen, S. G. and E. M. Kober. (2004). The generalized interpolation material point method. *Computer Modeling in Engineering & Sciences*, 5:477–496, 2004.

Bengtsson, R. Afshar, and E. K. Gamstedt. (2020). A basic orthotropic viscoelastic model for composite and wood materials considering available experimental data and time-dependent Poisson's ratios. *IOP Conference Series: Materials Science and Engineering*, 942:012021, 2020.

Beyreuther, I. Ganguly, M. Hoffman. (2017). CLT Demand Study for the Pacific Northwest, https://forterra.org/wp-content/uploads/2017/02/Pacific-NW-CLT-Demand-Study-December-2016.pdf

Boje, C., Guerriero, A., Kubicki, S., & Rezgui, Y. (2020). Towards a semantic Construction Digital Twin: Directions for future research. *Automation in Construction*, *114*, 103179.

Borodin, O., Bedrov, D., Smith, G.D., Nairn, J., Bardenhagen, S. (2005) Multiscale modeling of viscoelastic properties of polymer nanocomposites. Journal of Polymer Science, 43 pp. 1005-1013.

Boyd, J. D. (1982). An Anatomical Explanation for Visco-Elastic and Mechano-Sorptive Creep in Wood and Effects of Loading Rate on Strength. New Perspectives in Wood Anatomy.

Brandner, R. (2014). Production and Technology of Cross Laminated Timber (CLT): A State-of-the-Art Report. *Focus Solid Timber Solutions - European Conference on Cross Laminated Timber (CLT)*, no. May 2013: 3–36.

Buchanan, A.H., John, S., Love, S. (2013). LCA and carbon footprint of multi-story timber buildings compared with steel and concrete buildings. *N. Z. J. For. 57*, 9–18.

Chen. J, Bulbul. T, Taylor. J. E., and Olgun. G. (2014). A Case Study of Embedding Real-time Infrastructure Sensor Data to BIM. Construction Research Congress, ASCE, pp. 296-278, 2014.

Clouser, W. S. (1959). Creep of small wood beams under constant bending load.

Davies, M., and Fragiacomo, M. (2011). Long-term behavior of prestressed LVL members. I: Experimental tests. *J Struct Eng*, *137*(12), 1553-1561.

Desogus, G., Quaquero, E., Rubiu, G., Gatto, G., & Perra, C. (2021). BIM and IoT Sensors Integration: A Framework for Consumption and Indoor Conditions Data Monitoring of Existing Buildings. *Sustainability*, *13*(8), 4496.

Findley, W. N. and Davis, F. A. (2013). Creep and relaxation of nonlinear viscoelastic materials. Courier Corporation.

Florisson, S., Muszynski, L., and Vessby, J. (2021). Analysis of hygro-mechanical behavior of wood in bending. *Wood and Fiber Science*, *53*(1), 27-47.

Forest Products Laboratory. (2010) Forest Service, United States Department of Agriculture. Wood Handbook: Wood as an Engineering Material. Madison, WI, U.S. Dept. of Agriculture, Forest Service, Forest Products Laboratory.

Fortino, S., Mirianon, F., and Toratti, T. (2009). A 3d moisture-stress fem analysis for time dependent problems in timber structures. Mechanics of Time- Dependent Materials, 13(4), 333–356.

Frandsen, H.L., Damkilde, L. and Svensson, S. (2007). A revised multi-Fickian moisture transport model to describe non-Fickian effects in wood, vol. 61, no. 5, pp. 563-572. https://doi.org/10.1515/HF.2007.085

Freres Lumber Co., Inc. (2021). Mass Plywood Panel Certified by APA. Accessed on August 19th, 2021. https://frereslumber.com/blog/mass-plywood-panel-certified-by-apa/

Fridley, K. J., R. C. Tang, and L. A. Soltis. (1992a). Creep behavior model for structural lumber. Journal of Structural Engineering. 118 (8): 2261–2277. ASCE. 0733-9445(1992)118:8(2261). 1992.

Gallaher, M., O'Connor, A., Dettbarn, J., Jr., and Gilday, L. (2004). Cost analysis of inadequate interoperability in the US capital facilities industry. NIST Publication GCR 04-867, National Institute of Standards and Technology (NIST), Gaithersburg, MD.

Gerhards, C. C. (1985). Time-dependent bending deflections of Douglas-fir 2 by 4's. *Forest Products Journal*, *35*(4), 18-26.

Glass, S.V., S.L. Zelinka. (2010). Moisture Relations and Physical Properties of Wood, Forest Products Laboratory, Madison, WI.

Godinho, M., Machete, R., Ponte, M., Falcão, A., Gonçalves, A., Bento, R., (2020). BIM as a resource in heritage management: An application for the National Palace of Sintra, Portugal, Journal of Cultural Heritage, Volume 43, 2020, Pages 153-162, ISSN 1296-2074, https://doi.org/10.1016/j.culher.2019.11.010.

Granello, G., Broccardo, M., Palermo, A., & Pampanin, S. (2020). Fragility-based methodology for evaluating the time-dependent seismic performance of post-tensioned timber frames. *Earthquake Spectra*, *36*(1), 322-352.

Granello, G., C. Leyder, A. Palermo, A. Frangi, S. Pampanin. (2018). Design approach to predict post-tensioning losses in post-tensioned timber frames, J. Struct. Eng. 144 (8) 04018115, https://doi.org/10.1061/(ASCE)ST.1943-541X.0002101.

Granello, G., Leyder, C., Frangi, A., Palermo, A., & Chatzi, E. (2019). Long-term performance assessment of an operative post-tensioned timber frame structure. *Journal of Structural Engineering*, *145*(5), 04019034.

Granello, G., and Palermo, A. (2020). Monitoring Dynamic Properties of a Pres-Lam Structure: Trimble Navigation Office. Journal of Performance of Constructed Facilities 34 (1): 1–12. https://doi.org/10.1061/(ASCE)CF.1943-5509.0001359.

Granello, G., Palermo, A, Pampanin, S., Pei, S., van de Lint, J.W. (2020). "Pres-Lam buildings: state of the Art." *J. Struct. Eng*. 146 (6).

Grieves, M. (2014). Digital Twin: Manufacturing Excellence Through Virtual Factory Replication, White Paper, https://www.researchgate.net/publication/275211047

Grossman, P. U. A. (1978). Mechano Sorptive Behaviour. General Constitutive Relations of Wood and Wood-Based Materials.

Guo, N. (2009). Hygro-mechanical response of clear softwood specimens to compression under cyclic climate. MS Thesis. Oregon State University.

Hoffmeyer, P., Davidson, R.W. (1989). Mechano-sorptive creep mechanism of wood in compression and bending. *Wood Science and Technology.* 23, 215–227.

Holzer, S. M., Loferski, J. R., & Dillard, D. A. (1989). A review of creep in wood:

concepts relevant to develop long-term behavior predictions for wood structures. *Wood and Fiber Science*, *21*(4), 376-392.

Hoyle, R. J., Griffith, M. C., & Itani, R. Y. (1985). Primary creep in Douglas-fir beams of commercial size and quality. *Wood and Fiber Science*, *17*(3), 300-314.

Huč, S., & Svensson, S. (2018). Coupled two-dimensional modeling of viscoelastic creep of wood. *Wood Science and Technology*, *52*(1), 29-43.

Hu, L., Pirvu, C., and Ramzi, R. (2015). In-Situ Testing at Wood Innovation and Design Centre: Flor Vibration, Building Vibration, and Sound Insulation Performance. FPInnovations.

Hu, W.G., and Guan, H. (2018). Experimental and numerical investigation on compression creep behavior of wood. *Forest Products Journal*, 68(2):138–146.

Ikegami, K. (2001). Section 2.5 - Background on Viscoelasticity, Handbook of Materials Behavior Models, Academic Press, Pages 95-106, ISBN 9780124433410, https://doi.org/10.1016/B978-012443341-0/50010-7.

International Organization for Standardization (ISO). (2018). ISO 16739-1:2018 Industry Foundation Classes (IFC) for Data Sharing in the Construction and Facility Management Industries—Part 1: Data Schema, https://www.iso.org/standard/ 70303.html.

Kelly, J.M., Skinner, R.I. and Heine, A.J. (1974). Mechanism of Energy Absorption in Special Devices for Use in Earthquake Resistant Structures. Bulletin of the New Zealand Society of Earthquake Engineering, 5(3): 63-88

Kritzinger, W., M. Karner, G. Traar, J. Henjes, and W. Sihn, (2018). Digital Twin in manufacturing: A categorical literature review and classification. IFAC-PapersOnLine, vol. 51, no. 11, pp. 1016– 1022.

Lamb, K. (2019). Principle-based digital twins: a scoping review. https://doi.org/10.17863/CAM.47094

Leica Geosystems AG. (2021). Leica Cyclone 3D Point Cloud Processing Software. Accessed: April 12th, 2021. https://leica-geosystems.com/en-us/products/laser-scanners/software/leica-cyclone

Leica Geosystems AG. (2021). Leica CloudWorx for Revit. Accessed: April 9th, 2021.https://leica-geosystems.com/en-us/products/laser-scanners/software/leica-cloudworx/leica-cloudworx-revit

Leica Geosystems AG. (2021). Leica ScanStation P40/P30 – High-Definition 3D Laser Scanning Solution. Accessed: April 9th, 2021. https://leica-geosystems.com/en-us/products/laser-scanners/scanners/leica-scanstation-p40--p30.

Li, H.-N., L. Ren, Z.-G. Jia, T.-H. Yi, D.-S. Li. (2016). State-of-the-art in structural health monitoring of large and complex civil infrastructures, Journal of Civil. Struct. Health Monit. 6 (1) (2016) 3–16.

Longman, R.P., Baas, J., Turkan, Y., Riggio, M. (in press). Towards a digital twin for monitoring in-service performance of post-tensioned self-centering cross-laminated timber shear walls. *ASCE*. 2021.

Lu, Q., Chen, L., Li, S., & Pitt, M. (2020). Semi-automatic geometric digital twinning for existing buildings based on images and CAD drawings. *Automation in Construction*, *115*(February), 103183. https://doi.org/10.1016/j.autcon.2020.103183

Lu, Q., Xie, X., Heaton, J., Parlikad, A. K., & Schooling, J. (2019). From BIM towards digital twin: Strategy and future development for smart asset management. In *International Workshop on Service Orientation in Holonic and Multi-Agent Manufacturing* (pp. 392-404). Springer, Cham.

Macchi, M., Roda, I., Negri, E., Fumagalli, L. (2018). Exploring the role of digital twin for asset lifecycle management. IFAC-PapersOnLine. 2018 Jan 1;51(11):790-5.

Martynenko, V. G., & Lvov, G. I. (2017). Numerical prediction of temperature-dependent anisotropic viscoelastic properties of fiber reinforced composite. *Journal of Reinforced Plastics and Composites*, *36*(24), 1790-1801.

Mascia, N. T., & Lahr, F. A. R. (2006). Remarks on orthotropic elastic models applied to wood. *Materials Research*, *9*(3), 301-310.

Mohammadi N., J.E. Taylor. (2017). Smart city digital twins, IEEE Symposium Series on Computational Intelligence (SSCI), IEEE 2017. 1–5.

Morlier, P. (2004). Creep Timber Struct, 8. CRC Press.

Morrell, I., Soti, R., Miyamoto, B., & Sinha, A. (2020). Experimental investigation of base conditions affecting seismic performance of mass plywood panel shear walls. *Journal of Structural Engineering*, *146*(8), 04020149.

Morris, Hugh, Maggie Zhu, Michelle Wang. (2011). The Long Term Instrumentation of the NMIT Arts Building-Expan Shear Walls. NZ Timber Design Journal 20(1)13–24.

Muszyński, L., R. Lagaňa, W. Davids, and S.M. Shaler. (2005). Comments on the experimental methodology for quantitative determination of the hygro-mechanical properties of wood. Holzforschung, 59(2): 232-239.

Muszyński L. (2021). Glossary of terms. Unpublished course materials. Oregon State University.

Nairn, J.A. (2003). Material point method calculations with explicit cracks. *Computer Modeling in Engineering & Sciences*, 4:649–664, 2003.

Nairn, J.A., (2021). Material point method (NairnMPM, OSParticulas) and finite element analysis (NairnFEA) open-source software. http://osupdocs.forestry.oregonstate.edu/. Oregon State University, Corvallis, Oregon. 2021.

Nairn, J. A., and C. C. Hammerquist. (2021). Material point method simulations using an approximate full mass matrix inverse. *Computer Methods in Applied Mechanics and Engineering*, 377:113667.

Nairn, J. A., S. G. Bardenhagen, and G. S. Smith. (2018). Generalized contact and improved frictional heating in the material point method. *Computational Particle Mechanics*, 5(3):285–296. 2018.

Nallainathan, L., Liu, X. L., Chiu, W. K., & Jones, R. (2004). Modelling creep behaviour of orthotropic composites by the coincident element method. *Composite structures*, *66*(1-4), 409-413.

Napolitano R, Blyth A, and Glisic B. (2018). Virtual Environments for Visualizing Structural Health Monitoring Sensor Networks, Data, and Metadata. *Sensors an Open Access Journal from MDPI.*

Nguyen, T. T., Dao, T. N., Aaleti, S., Hossain, K., & Fridley, K. J. (2019). Numerical model for creep behavior of axially loaded CLT panels. *Journal of Structural Engineering*, *145*(1), 04018224.

Niemz, P., Mannes, D. (2012). Non-destructive testing of wood and wood-based materials, Journal of Cultural Heritage, Volume 13, Issue 3, Supplement, 2012, Pages S26-S34, ISSN 1296-2074, https://doi.org/10.1016/j.culher.2012.04.001.

NOAA. (2021). What is lidar? National Ocean Service website. Accessed April 12, 2021. https://oceanservice.noaa.gov/facts/lidar.html

Open Science Framework. (2021). Peavy Hall – Structural health monitoring data under construction. Accessed April 12th, 2021. https://osf.io/jdz6y/

Palermo, A., S. Pampanin, A. Buchanan, and M. Newcombe. (2005). Seismic design of multi-storey buildings using laminated veneer lumber (LVL). In Proc., NZ Society EQ Eng Conf. Wairakei, New Zealand.

Pei, S., van de Lindt, J.W., Barbosa, A.R., Berman, J., McDonnell, E., Dolan, J.D., Blomgren, H., Zimmerman, E., Huang, D., Wichman, S. (2019). Experimental Seismic Response of a Resilient 2-Story Mass-Timber Building with Post-Tensioned Rocking Walls. *ASCE J Struct Eng*. 145(11).

Pocobelli, D.P., Boehm, J., Bryan, P., Still, J., and Grau-Bove, J. (2018). BIM for heritage science: a review. *Heritage Science* **6,** 30. https://doi.org/10.1186/s40494-018-0191-4

Riggio, M., Anthony, R.W., Augelli, F., Kasal, B., Lechner, T., Muller, W., Tannert, T. (2014). In situ assessment of structural timber using non-destructive techniques. *Mater Struct* **47,** 749–766 (2014). https://doi.org/10.1617/s11527-013-0093-6

Rio, J., Ferreira B. and Pocas Martins J, (2013). Expansion of IFC model with structural sensors, J. Informes de la Construccion, ISSN: 0020-0883, Vol. 65, no. 530, pp. 219-228, 2012.

Schänzlin, J. (2010). Modeling the long-term behavior of structural timber for typical service class-II conditions in South-West Germany. University of Stuttgart.

Schulitz, Helmut C., Sobek, W., and Habermann, K.J. (2012). *Steel Construction Manual*. Walter de Gruyter.

Senft, J. F., & Suddarth, S. K. (1971). An analysis of creep-inducing stress in Sitka spruce. *Wood and Fiber Science*, *2*(4), 321-327.

Sepasgozar, S.M.E. (2021). Differentiating Digital Twin from Digital Shadow: Elucidating a Paradigm Shift to Expedite a Smart, Sustainable Built Environment. Buildings 2021, 11, 151. https://doi.org/10.3390/buildings11040151

Shafto, M., Conroy, M., Doyle, R., Glaessgen, E., Kemp, C., LeMoigne, J., & Wang, L. (2012). Modeling, Simulation, information Technology & Processing Roadmap. In *Technology Area 11*.

Shalabi, F., and Turkan, Y. (2017). IFC BIM-based facility management approach to optimize data collection for corrective maintenance. *Journal of performance of constructed facilities*, *31*(1), 04016081.

Siau, J. F. (1984). Transport processes in wood (Vol. 2). Springer Science & Business Media.

Skaar, C. (1988). Wood-Water Relations. *Springer Series in Wood Science*.

Smith, T., Sarti, F., Granello, G., Marshall, J., Buckton-Wishart, V., Li, M., Palermo, A., & Pampanin, S. (2016). Long-term dynamic characteristics of pres-lam structures. World Conference on Timber Engineering (WCTE).

Smith, T., Ponzo, F., Di Cesare, A., Pampanin, S., Carradine, D., Buchanan, A., and Nigro, D. (2014). Post-Tensioned Glulam Beam-Column Joints with Advanced Damping Systems: Testing and Numerical Analysis, Journal of Earthquake and Engineering, 18:1, 147-167.

Sohn H., C.R. Farrar, F.M. Hemez, D.D. Shunk, D.W. Stinemates, B.R. Nadler, J.J. Czarnecki, D.D. Shunk, D.W. Stinemates, B.R. Nadler, J.J. Czarnecki. (2003). A Review of Structural Health Monitoring Literature: 1996–2001, Los Alamos National Laboratory.

Sulsky, D., Chen, Z., and Schreyer, H. L. (1994). A particle method for history-dependent materials. Computer Methods in Applied Mechanics and Engineering, 118(1–2), 179–196.

Suprabhas, K., and Hazar Nicholas, D. (2017). Integration of BIM and utility sensor data for facilities management. In *Computing in Civil Engineering 2017*, pp. 26-33.

Teicholz, P. (2013). BIM for Facility Managers; John Wiley & Sons: Hoboken, NJ, USA.

Theiler M., K. Smarsly. (2018). IFC Monitor – An IFC schema extension for modeling structural health monitoring systems, Advanced Engineering Informatics, Volume 37, Pages 54-65, ISSN 1474-0346, https://doi.org/10.1016/j.aei.2018.04.011.

Toratti, T. (1992). Creep of timber beams in a variable environment, Dissertation, Helsinki University of Technology, VTT, Espoo.

Tuegel, E.J., A.R. Ingraffea, T.G. Eason, S.M. Spottswood. (2011). Reengineering aircraft structural life prediction using a digital twin, International Journal of Aerospace Engineering 2011, 1–14.

Valinejadshoubi, M., Bagchi, A., & Moselhi, O. (2017). Managing Structural Health Monitoring Data Using Building Information Modelling. Fourth Conference on Smart Monitoring, Assessment and Rehabilitation of Civil Structures, 1–10.

Vidal-Sallé, E., & Chassagne, P. (2007). Constitutive equations for orthotropic nonlinear viscoelastic behaviour using a generalized Maxwell model Application to wood material. *Mechanics of Time-Dependent Materials*, *11*(2), 127-142.

Yan, L., Zhaoxiang, S., Kai, D. (2015). Application of BIM in the protection of historical buildings based on Riegel historic value theory. *Atlantis Press.*

Zhang, J., Seet, B. C., & Lie, T. T. (2015). Building information modelling for smart built environments**.** Buildings, 5(1), 100–115.